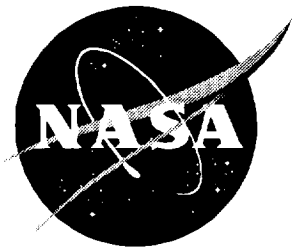

NASA Technical Paper 3623

Direct Numerical Simulation of Evolution and Control of Linear and Nonlinear Disturbances in Three-Dimensional Attachment-Line Boundary Layers

Ronald D. Joslin

February 1997

NASA Technical Paper 3623

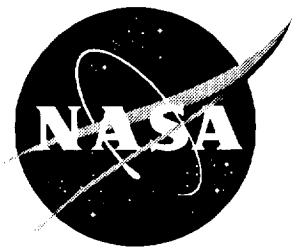

Direct Numerical Simulation of Evolution and Control of Linear and Nonlinear Disturbances in Three-Dimensional Attachment-Line Boundary Layers

Ronald D. Joslin
Langley Research Center • Hampton, Virginia

National Aeronautics and Space Administration
Langley Research Center • Hampton, Virginia 23681-0001

February 1997

Acknowledgments

R.-S. Lin, High Technology Corporation, Hampton, Virginia, provided the initial disturbance information for comparison with the Lin-Malik theory. J. R. Dagenhart, W. L. Sellers III, S. G. Anders, and F. J. Chen, of Langley Research Center, reviewed this paper.

Available electronically at the following URL address: http://techreports.larc.nasa.gov/ltrs/ltrs.html

Printed copies available from the following:

NASA Center for AeroSpace Information
800 Elkridge Landing Road
Linthicum Heights, MD 21090-2934
(301) 621-0390

National Technical Information Service (NTIS)
5285 Port Royal Road
Springfield, VA 22161-2171
(703) 487-4650

Contents

Tables

Figures

Symbols

A	amplitude of disturbance
A.L.	attachment line
$\mathbf{D}_y$	spectral wall-normal derivative operator
$\tilde{\mathbf{D}}_y$	derivative operators with the first and last rows set to zero
$\mathbf{D}_z$	flow-acceleration derivative operator
$\tilde{\mathbf{D}}_z$	derivative operators with the first and last rows set to zero
DNS	direct numerical simulation
E	disturbance energy
E_o	initial disturbance energy
$\mathbf{I}$	identity matrix
$\mathbf{I}_G^{GL}$	Gauss to Gauss-Lobatto point transform
$\mathbf{I}_{GL}^{G}$	Gauss-Lobatto to Gauss point transform
L	length scale along flow-acceleration direction
$\mathbf{L}_x$	attachment-line-directed central finite-difference operator
$\mathbf{L}_y$	wall-normal-directed spectral operator
$\mathbf{L}_z$	flow-acceleration-directed spectral operator
OS	Orr-Sommerfeld–Squire equations
P	mean-flow pressure component
P_o	pressure component at attachment line
p	disturbance pressure component
$\tilde{p}$	instantaneous pressure
$\mathbf{Q}$	eigenvector matrix of $\mathbf{L}_y$ operator
$\mathbf{Q}^{-1}$	inverse of $\mathbf{Q}$-matrix
R	Reynolds number, $\frac{U_o\delta}{\nu} = 2.475R_\theta$
R_θ	momentum-thickness Reynolds number, $\frac{U_o\theta}{\nu}$
RK	Runge-Kutta
$\mathbf{S}$	eigenvector matrix of $\mathbf{L}_z$ operator
$\mathbf{S}^{-1}$	inverse of $\mathbf{S}$-matrix
SB	unsteady suction and blowing location
t	time
$\underline{\mathbf{U}}$	mean-flow velocity vector, (U,V,W)
U,V,W	mean-flow attachment-line, wall-normal, and flow-acceleration velocities
U_o,V_o,W_o	velocity at boundary-layer edge of attachment line
U_∞	free-stream velocity
$\underline{\mathbf{u}}$	disturbance velocity vector, (u,v,w)
u,v,w	disturbance attachment-line, wall-normal, and flow-acceleration velocities
$\tilde{\underline{\mathbf{u}}}$	instantaneous velocities, $\underline{\mathbf{U}} + \underline{\mathbf{u}}$

$\hat{u},\hat{v},\hat{w}$	mean-flow attachment-line, wall-normal, and flow-acceleration similarity velocities
u_o,v_o	mean-flow distortion
X,Y,Z	nondimensional attachment-line, wall-normal, and flow-acceleration coordinates, $\frac{\{x,y,z\}}{\delta}$
$\underline{x}$	Cartesian coordinate system, (x,y,z)
x,y,z	attachment-line, wall-normal, and flow-acceleration coordinates
$Y_{\max}$	nondimensional wall-normal computational boundary location
$Z_{\max}$	nondimensional flow-acceleration computational boundary location
α	disturbance attachment-line wave number
α_i	attachment-line disturbance growth rate
α_r	attachment-line disturbance wave number
δ	length scale, $\sqrt{\nu L/W_o}$
κ	transpiration constant, $V_o\sqrt{L/\nu W_o}$
Λ_y	eigenvalue matrix of $\mathbf{L}_y$ operator
Λ_z	eigenvalue matrix of $\mathbf{L}_z$ operator
ν	fluid kinematic viscosity
ω	disturbance frequency
$\otimes$	tensor product
2D	two-dimensional
3D	three-dimensional
Subscript:	
max	maximum

1. Summary

The linear and the nonlinear stability of disturbances that propagate along the attachment line of a three-dimensional boundary layer is considered. The spatially evolving disturbances in the boundary layer are computed by direct numerical simulation (DNS) of the unsteady, incompressible Navier-Stokes equations. Disturbances are introduced either by forcing at the inflow or by applying suction and blowing at the wall. Quasi-parallel linear stability theory and a nonparallel theory yield notably different stability characteristics for disturbances near the critical Reynolds number; the DNS results confirm the nonparallel theory. The simulation results show that suction stabilizes the quasi-two-dimensional attachment-line disturbances, and blowing destabilizes these disturbances; these results qualitatively agree with the theory. Previously, a weakly nonlinear theory and computations revealed a high wave-number region of subcritical disturbance growth, which is a region where linear theory predicts the decay of small-amplitude disturbances. More recent computations have failed to achieve this subcritical growth. The present computational results duplicate and explain both subcritically growing and decaying disturbances. Furthermore, an explanation is provided for the previous theoretical and computational discrepancy. The present results demonstrate that steady suction can be used to stabilize disturbances that otherwise grow subcritically along the attachment line. However, true three-dimensional disturbances are more likely in practice and are more stable than two-dimensional disturbances. Disturbances generated off (but near) the attachment line spread both away from and toward the attachment line as they evolve. Furthermore, the results show that suction stabilizes the disturbances that develop off the attachment line. Clearly, disturbances that are generated near the attachment line can supply energy to attachment-line instabilities, but suction can be used to stabilize these instabilities. Finally, symmetric and asymmetric disturbance growth predicted by a two-dimensional-eigenvalue approach is demonstrated to agree with the DNS results.

2. Introduction

On a swept wing, many instability mechanisms occur that can lead to the catastrophic breakdown of laminar to turbulent flow. Contamination along the leading edge, Tollmien-Schlichting waves, stationary or traveling cross-flow vortices, Taylor-Görtler vortices, or combinations of these modes are among the mechanisms that can lead to this breakdown. For brevity, the discussion here is limited to disturbances in the region of the attachment line. For a more complete discussion of transition to turbulence on swept wings, refer to the work of Tuttle and Maddalon (1982), which includes a review of literature on laminar flow control, and of Reed and Saric (1986), which includes a description of the known physical mechanisms associated with transition. Koerner et al. (1987) present a German perspective on the laminarization of transport aircraft, and Gad-el-Hak and Bushnell (1991) discuss separation control on wings. The most recent and comprehensive overview of experiments, theory, and computations related to boundary-layer transition prediction and application to drag reduction is given by Arnal (1992).

Contamination at the leading edge results from turbulence at a fuselage-wing juncture, which travels out over the wing and contaminates otherwise laminar flow on the wing. If the Reynolds number of the attachment-line boundary layer is greater than some critical value, then this contamination inevitably leads to turbulent flow over the complete wing; this phenomenon has been demonstrated by Pfenninger (1965), Maddalon et al. (1990), and others. To correct this problem, Gaster (1965) placed a bump on the leading edge to prevent the turbulent attachment-line boundary layer from sweeping over the entire wing. This bump must be shaped to create a fresh stagnation point without generating a detrimental adverse pressure gradient. Outboard of the bump, a new laminar boundary layer forms.

Although the problem of turbulent flow that originates from the fuselage-wing juncture and contaminates the entire wing can be avoided by using a device such as the Gaster bump, a Reynolds number exists beyond which disturbances generated by surface imperfections or particulates on the wing, when combined with noise, will eventually cause transition. If we assume that the initiated disturbances are sufficiently small, hydrodynamic stability theory could potentially be used to predict the spatial amplification and the decay of the disturbances along the attachment line. Gaster (1967) first examined this small-amplitude disturbance problem by using acoustic excitation along the attachment line of a swept cylinder model. Gaster fed the flow sine waves with various frequencies that were detected by a hot-film gauge on the attachment line. He noted that the recorded oscillations had preferred frequency bands that changed with tunnel speed and that this behavior was similar to that of traveling-wave instabilities. From his measurements, he concluded that the small-amplitude disturbances in an attachment-line boundary layer were stable for momentum-thickness Reynolds numbers R_θ below 170 (the critical Reynolds number was outside the experimental range); this value for the critical Reynolds number is close to the theoretical value of 200, which is obtained by assuming a two-dimensional (2D) attachment-line boundary layer. Later, Cumpsty and

Head (1969) experimentally studied large-amplitude disturbances and turbulent flow along the attachment line of a swept-wing model. They observed that laminar flow is stable to small-amplitude disturbances up to $R_\theta \approx 245$ (which corresponds to the top speed of the tunnel). Cumpsty and Head note that this observation remains consistent with the theoretical value. At the same time, Pfenninger and Bacon (1969) used a wing swept to 45° to experimentally study the attachment-line instabilities in a wind tunnel that was capable of the larger speeds necessary to obtain unstable disturbances. With hot wires, they observed regular sinusoidal oscillations with frequencies comparable with the most unstable 2D modes of theory; these modes caused transition to occur at $R_\theta \approx 240$. A continued interest in transition initiated near the attachment line of swept wings led Poll (1979, 1980) to conduct additional experiments. With the swept circular cylinder model of Cumpsty and Head (1969), Poll defined criteria for the onset of turbulence and identified the forms of the disturbances present in the flow. Like Pfenninger and Bacon (1969), Poll observed disturbances that amplified along the attachment line. He noted that no unstable modes were observed below $R_\theta = 230$.

With an eigenvalue problem approach, Hall, Malik, and Poll (1984) studied the linear stability of disturbances in the attachment-line boundary-layer flow called "swept Hiemenz flow," which is illustrated in figure 2.1. This 3D base flow is a similarity solution to the Navier-Stokes equations; hence, its use is advantageous in stability analyses. By assuming periodic disturbance modes along the attachment line, Hall, Malik, and Poll (1984) determined neutral curves with and without the presence of steady suction and demonstrated that the attachment-line boundary layer theoretically can be stabilized with small amounts of suction. Hereafter the Hall, Malik, and Poll (1984) approach is referred to as a "nonparallel theory" because the study accounted for all linear terms, including the wall-normal velocity component of the base flow. Spalart (1989) used a direct numerical simulation (DNS) approach, based on the fringe method, to study the leading-edge contamination problem. Small-amplitude disturbances were initialized with white noise. Reynolds number test points were selected in both the stable and unstable regime to assess the validity of the nonparallel theory by Hall, Malik, and Poll (1984). At the lower Reynolds number, all disturbances decayed; at the higher number, at least one mode was amplified. The critical Reynolds number predicted by Hall, Malik, and Poll (1984) fell within the Reynolds number range used by Spalart; the results of the simulations indicate good qualitative agreement with the linear theory. Furthermore, Spalart (1989) demonstrated that classical Hiemenz flow is stable to both linear and nonlinear modes. Theofilis (1993a) performed DNS of the 2D linear disturbances that propagate along the attachment line of swept Hiemenz flow; the DNS results agreed with Hall, Malik, and Poll (1984) near branch II of the neutral curve but were in disagreement near branch I. Theofilis (1993a) attributed this disagreement between DNS and theory to a lack of DNS grid resolution near branch I. Small-amplitude DNS computations by Jiménez et al. (1990) led to results that agreed with the linear results of Hall, Malik, and Poll (1984) for both branch I and branch II of the neutral curve.

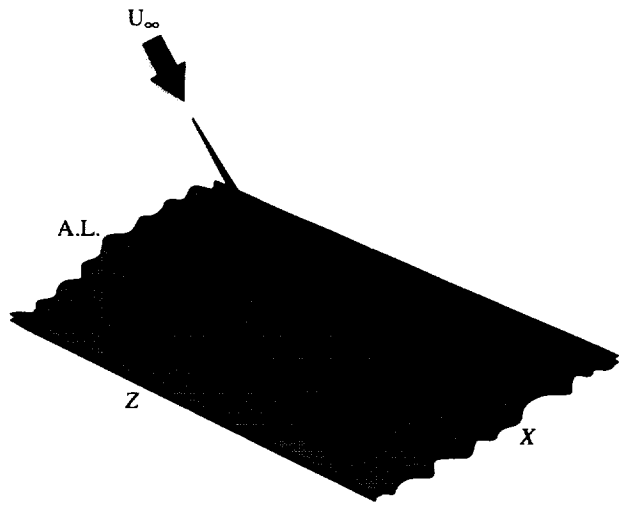

Figure 2.1. Sketch of attachment-line region of swept Hiemenz flow.

In summary, table 2.1 shows that both the experiments and calculations agree (approximately) for the critical Reynolds number at which small-amplitude disturbances begin to amplify.

As the initial amplitude of the disturbances in the attachment-line region become large, the experimental results show considerable discrepancy between the onset of transition and the linear critical Reynolds number. Pfenninger and Bacon (1969) placed a wire upstream of the attachment line and generated large-amplitude

Table 2.1. Experimental and Theoretical Critical Points for Linear Instabilities in Attachment-Line Boundary Layers

Reference	Critical R_θ
Experiment	
Cumpsty and Head 1969	245
Pfenninger and Bacon 1969	240
Poll 1979, 1980	230
Theory	
Hall, Malik, and Poll 1984	245

fluctuations in the boundary layer. They observed transition at $R_\theta = 155$. In his study of leading-edge contamination, Pfenninger (1965) discovered through in-flight experiments that laminar flow could be obtained for $R_\theta < 100$; for $R_\theta > 100$, leading-edge contamination occurred. In their wind-tunnel experiments on a swept airfoil, Gregory and Love (1965) found that for $R_\theta > 95$ complete turbulence occurred. Flight tests by Gaster (1967) showed that turbulent spots were first present at $R_\theta > 88$. Cumpsty and Head (1969) and later Poll (1985) used a swept model in a wind tunnel to show that turbulence was damped for $R_\theta < 99$ and that the leading edge was fully turbulent for $R_\theta > 114$. Namely, for $R_\theta < 100$, disturbances are damped (turbulence decay), and for $R_\theta > 100$, the flow becomes turbulent (note the wide gap between the linear critical Reynolds number of $R_\theta \approx 245$ and the turbulent-decay Reynolds number of $R_\theta \approx 100$). Table 2.2 summarizes the experimental results which indicate the Reynolds number when turbulence no longer decays and can fully contaminate the attachment-line flow.

Table 2.2. Experimental Critical Points for Turbulence Suppression in Attachment-Line Boundary Layers

Experiment	Bypass R_θ
Pfenninger 1965	100
Gregory and Love 1965	95–98
Gaster 1967	88–104
Cumpsty and Head 1969	100
Poll 1985	100

Hall and Malik (1986) strived to bridge the gap between the nonparallel linear theory and bypass transition Reynolds numbers by studying large-amplitude disturbances with weakly nonlinear theory and temporal DNS. They note that subcritical disturbance growth is observed at wave numbers that correspond to branch II of the neutral curve. Consistent with the experimental results, large-amplitude disturbances become unstable before the linear critical point and approach equilibrium states near branch I of the neutral curve. Both Jiménez et al. (1990) and Theofilis (1993b) failed to find this region of subcritical growth with a temporal DNS code. Jiménez et al. (1990) contend that this subcritical growth region does not exist.

Using asymptotic analysis, Hall and Seddougui (1990) studied oblique waves and their interaction in attachment-line flow at the large Reynolds number limit. They note that close to the attachment line a small band of destabilized oblique modes appear, interact with the 2D mode, and cause a breakdown of the 2D mode. In addition, they note that oblique modes become less important away from the attachment line and that low-frequency modes become the dominant mechanism (i.e., stationary cross-flow modes). Lin and Malik (1994) performed 3D linear computations which showed that, in addition to the dominant 2D symmetric wave (studied here), both asymmetric and symmetric modes can be unstable depending on the Reynolds number. Hence, evidence of 3D modes on or near the attachment line has theoretically been demonstrated.

Bridging the understanding of the gap between the Reynolds number region of linear instability (table 2.1) and the lower Reynolds number region where turbulence is suppressed (table 2.2) is important for nacelle and swept-wing design. As a first step toward understanding this inherently nonlinear 3D process, the present study focuses on validating the linear theories, studying the nonlinear subcritically growing disturbances, and examining 3D linear disturbances on and off the attachment line.

In section 3, the physical and mathematical description of the problem is formulated. In sections 4 and 5, a well-tested 3D spatial DNS code described by Joslin, Streett, and Chang (1992, 1993) is used to independently study both the linear and nonlinear instabilities that initiate and develop along the attachment line of a swept Hiemenz flow. Regions near both branches (I and II) of the neutral curve are investigated with DNS to simultaneously verify the form of the disturbances used in the DNS and the nonparallel theory (eigenvalue approach) of Hall, Malik, and Poll (1984) for infinitesimal disturbances. A resolution to the discrepancy between the weakly nonlinear theory and supporting computations by Hall and Malik (1986) and the two recent DNS computations is described in section 5. Furthermore, steady suction is used to control the nonlinear disturbance growth. Finally, section 6 describes a newly developed 3D DNS code (which has no approximation for periodicity) and presents results for symmetric and asymmetric disturbances generated on and off (but near) the attachment line.

3. Problem Formulation

In general, the velocities $\tilde{\mathbf{u}} = (\tilde{u},\tilde{v},\tilde{w})$ and the pressure $\tilde{p}$ are solutions of the incompressible, unsteady Navier-Stokes equations. The instantaneous velocities $\tilde{\mathbf{u}}$ and the pressure $\tilde{p}$ may be decomposed into base and disturbance components as

$$\left.\begin{aligned} \tilde{\mathbf{u}}(\underline{x},t) &= \underline{\mathbf{U}}(\underline{x}) + \underline{\mathbf{u}}(\underline{x},t) \\ \tilde{p}(\underline{x},t) &= P(\underline{x}) + p(\underline{x},t) \end{aligned}\right\} \qquad (3.1)$$

where the base flow is given by the velocities $\underline{\mathbf{U}} = (U,V,W)$ and the pressure P, and the disturbance

component is given by the velocities $\underline{u} = (u,v,w)$ and the pressure p. A Cartesian coordinate system $\underline{x} = (x,y,z)$ is used in which x is aligned with the attachment line, y is wall normal, and z corresponds to the direction of flow acceleration away from the attachment line.

3.1. Base Component

The mean, or base, flow of interest is referred to as swept Hiemenz flow. Shown in figure 2.1, the fluid comes obliquely down toward the wall; it turns away from the attachment line into the $\pm z$-directions to form a boundary layer. In the x-direction, the flow is uniform. In the absence of sweep, U_o is equal to 0 and the flow reduces to the 2D stagnation flow first described by Hiemenz (1911). Where U_o, V_o, W_o are velocity scales, and L is the length scale in the flow-acceleration direction Z, a length scale (factor of the boundary-layer thickness) is defined in the YZ-plane as $\delta = \sqrt{\nu L/W_o}$; a Reynolds number, as $R = U_o\delta/\nu = 2.475R_\theta$; and a transpiration constant, as $\kappa = V_o\sqrt{L/\nu W_o}$, where $\kappa = 0$ for the zero-suction case. If the attachment line is assumed to be infinitely long, the velocities become functions of Z and Y only, and the similarity solution can be found.

The swept Hiemenz formulation was originally described by Hall, Malik, and Poll (1984), where a linear stability analysis of the flow was performed. The respective velocities and pressure for swept Hiemenz flow are $\{U,V,W,P\}$ and the governing equations are given as

$$\frac{\partial U}{\partial X} + \frac{\partial V}{\partial Y} + \frac{\partial W}{\partial Z} = 0 \tag{3.2}$$

$$U\frac{\partial U}{\partial X} + V\frac{\partial U}{\partial Y} + W\frac{\partial U}{\partial Z} = -\frac{\partial P}{\partial X} + \frac{1}{R}\left(\frac{\partial^2 U}{\partial X^2} + \frac{\partial^2 U}{\partial Y^2} + \frac{\partial^2 U}{\partial Z^2}\right) \tag{3.3}$$

$$U\frac{\partial V}{\partial X} + V\frac{\partial V}{\partial Y} + W\frac{\partial V}{\partial Z} = -\frac{\partial P}{\partial Y} + \frac{1}{R}\left(\frac{\partial^2 V}{\partial X^2} + \frac{\partial^2 V}{\partial Y^2} + \frac{\partial^2 V}{\partial Z^2}\right) \tag{3.4}$$

$$U\frac{\partial W}{\partial X} + V\frac{\partial W}{\partial Y} + W\frac{\partial W}{\partial Z} = -\frac{\partial P}{\partial Z} + \frac{1}{R}\left(\frac{\partial^2 W}{\partial X^2} + \frac{\partial^2 W}{\partial Y^2} + \frac{\partial^2 W}{\partial Z^2}\right) \tag{3.5}$$

where the equations are nondimensionalized with respect to the attachment-line velocity U_o, the length scale δ, and the kinematic viscosity ν.

A mean, or steady, solution of the Navier-Stokes equations is sought that obeys the following conditions:

At the wall, we require that

$$\left.\begin{aligned} U = W = 0 \\ V = V_o \end{aligned}\right\} \quad (y = 0) \tag{3.6}$$

and sufficiently far away from the wall,

$$\left.\begin{aligned} U \to U_o \\ W \to W_o\frac{z}{L} \end{aligned}\right\} \quad (y \to \infty) \tag{3.7}$$

The velocity field for this similarity solution is

$$\left.\begin{aligned} U(Y) &= \hat{u}(Y) \\ V(Y) &= \frac{1}{R}\hat{v}(Y) \\ W(Y,Z) &= \frac{Z}{R}\hat{w}(Y) \end{aligned}\right\} \tag{3.8}$$

Substituting the nondimensional velocities (eqs. (3.8)) into the Z momentum equation (3.5) results in

$$\frac{Z}{R^2}\hat{v}\frac{d\hat{w}}{dY} + \frac{Z}{R^2}\hat{w}^2 = -\frac{\partial P}{\partial Z} + \frac{Z}{R^2}\frac{d^2\hat{w}}{dY^2} \tag{3.9}$$

As $Y \to \infty$, the Z momentum equation (3.9) reduces to

$$\frac{Z}{R^2} = -\frac{\partial P}{\partial Z} \tag{3.10}$$

Integrating equation (3.10), we can infer that the required pressure form satisfying equations (3.7) is

$$P = P_o - \frac{1}{2}\frac{Z^2}{R^2} \tag{3.11}$$

where P_o is the constant pressure at the attachment line.

Substitute the velocity form (eqs. (3.8)) and the pressure form (eq. (3.11)) into the Navier-Stokes equations (eqs. (3.2)–(3.5)). Then by substituting the continuity equation into the momentum equations and subtracting

the Y and Z momentum equations, the following ordinary differential equation system for $\hat{u},\hat{v},\hat{w}$ results:

$$\hat{w} + \frac{d\hat{v}}{dY} = 0 \tag{3.12}$$

$$\frac{d^2\hat{u}}{dY^2} - \hat{v}\frac{d\hat{u}}{dY} = 0 \tag{3.13}$$

$$\frac{d^3\hat{v}}{dY^3} + \left(\frac{d\hat{v}}{dY}\right)^2 - \hat{v}\frac{d^2\hat{v}}{dY^2} - 1 = 0 \tag{3.14}$$

subject to the boundary conditions given by

$$\left.\begin{aligned} \frac{d\hat{v}}{dY} &= 0 \\ \hat{v} &= \kappa \\ \hat{w} &= 0 \end{aligned}\right\} \quad (Y = 0) \tag{3.15}$$

$$\left.\begin{aligned} \frac{d\hat{v}}{dY} &\to -1 \\ \hat{w} &\to 1 \end{aligned}\right\} \quad (Y \to \infty) \tag{3.16}$$

In the absence of sweep, equations (3.12)–(3.16) reduce to the famous 2D stagnation flow as first described by Hiemenz (1911).

Note that in the character of this similarity solution, U and V are uniform along the attachment line and W varies linearly with distance from the attachment line. Because of the properties of this base flow, both temporal and spatial DNS approaches should yield equivalent results in the 2D limit for small-amplitude disturbances. However, the temporal DNS assumes that disturbances are growing in time and that there exists a linear transformation from temporal growth to the realistic spatially growing instabilities. Hall and Malik (1986) realized subcritically growing instabilities with a temporal DNS code, and hence the difference between the weakly nonlinear theory and the previous computations should not be attributable to the temporal DNS approximation. Although many previous studies have made use of the temporal approach because of the computational savings over the spatial formulation, the spatial and temporal formulations are only related in the linear limit, with the spatial formulation being more representative of the true physical problem.

3.2. Disturbance Component

The disturbance portion of equations (3.1) is found by solving the 3D incompressible Navier-Stokes equations in disturbance form as

$$\frac{\partial u}{\partial t} + (U+u)\frac{\partial u}{\partial X} + (V+v)\frac{\partial u}{\partial Y} + (W+w)\frac{\partial u}{\partial Z} + (V+v)\frac{\partial U}{\partial Y} = -\frac{\partial p}{\partial X} + \frac{1}{R}\left(\frac{\partial^2 u}{\partial X^2} + \frac{\partial^2 u}{\partial Y^2} + \frac{\partial^2 u}{\partial Z^2}\right) \tag{3.17}$$

$$\frac{\partial v}{\partial t} + (U+u)\frac{\partial v}{\partial X} + (V+v)\frac{\partial v}{\partial Y} + (W+w)\frac{\partial v}{\partial Z} + (V+v)\frac{\partial V}{\partial Y} = -\frac{\partial p}{\partial Y} + \frac{1}{R}\left(\frac{\partial^2 v}{\partial X^2} + \frac{\partial^2 v}{\partial Y^2} + \frac{\partial^2 v}{\partial Z^2}\right) \tag{3.18}$$

$$\frac{\partial w}{\partial t} + (U+u)\frac{\partial w}{\partial X} + (V+v)\frac{\partial w}{\partial Y} + (W+w)\frac{\partial w}{\partial Z} + (V+v)\frac{\partial W}{\partial Y} + w\frac{\partial W}{\partial Z} = -\frac{\partial p}{\partial Z} + \frac{1}{R}\left(\frac{\partial^2 w}{\partial X^2} + \frac{\partial^2 w}{\partial Y^2} + \frac{\partial^2 w}{\partial Z^2}\right) \tag{3.19}$$

with the continuity equation and boundary conditions

$$\left.\begin{aligned} u &= 0 \qquad (Y = 0) \\ u &\to 0 \qquad (Y \to \infty) \end{aligned}\right\} \tag{3.20}$$

4. Attachment-Line Disturbances for 2D Assumption

4.1. Form of Disturbances

In general, disturbances on and near a 3D attachment-line region are of the 3D nature and require solutions of the full 3D Navier-Stokes equations. However, as assumed in the original theoretical study by Hall, Malik, and Poll (1984) and confirmed in the DNS computations by Spalart (1989), a single mode in the attachment-line region of swept Hiemenz flow can take the form that had a linear variation of the chordwise velocity component with distance from the attachment line. In the present study, an alternate disturbance form is first used. Namely, the velocity component w of the disturbance and the transverse shear of the mean flow are negligible; the disturbance becomes truly 2D along the attachment line. This condition implies that $w = 0$ and $\partial w/\partial Z = 0$ on the attachment line. Although this simplification is not consistent with the equations of motion, it turns out that the neglected terms have little effect on the qualitative behavior of the computed disturbances. This assumption allows us to use a preexisting DNS

solver, which has been tested for 2D instabilities and 3D spanwise periodic disturbances in 2D and 3D base flows. This 2D assumption is arguably valid because the flow is overwhelming dominated by the flow in the attachment-line direction.

4.2. Numerical Methods of Solution

A well-tested 3D spatial DNS code described by Joslin, Streett, and Chang (1992, 1993) is used to independently study both the linear and nonlinear instabilities that initiate and develop along the attachment line of a swept Hiemenz flow.

In the attachment-line (X) direction, fourth-order central finite differences are used for the pressure equation and sixth-order compact differences are used for the momentum equations in the interior of the computational domain. At the boundary and near-boundary nodes, fourth-order forward and backward differences are used. The discretization yields a pentadiagonal system for the finite-difference scheme and a tridiagonal system for the compact-difference scheme. The approximations can be solved efficiently by appropriate backward and forward substitutions.

In the wall-normal (Y) direction, the Chebyshev series is used to approximate the disturbances at Gauss-Lobatto collocation points. A Chebyshev series is used in the wall-normal direction because it provides good resolution in the high-gradient regions near the boundaries. Furthermore, the use of as few grid points as possible results in significant computational cost savings. In particular, the use of the Chebyshev series enables an efficient pressure solver. Because this series and its associated spectral operators are defined on $[-1,1]$ and the physical problem of interest has a truncated domain $[0,Y_{max}]$, a transformation is employed. Furthermore, a stretching function is used to cluster the grid near the wall. For further details on the properties and the use of spectral methods, refer to Canuto et al. (1988).

For time marching, a time-splitting procedure was used with implicit Crank-Nicolson differencing for normal diffusion terms; an explicit three-stage Runge-Kutta (RK) method by Williamson (1980) was used for the remaining terms. For details of the time-marching procedure, refer to Joslin, Streett, and Chang (1992). The intermediate RK velocities are determined semi-implicitly, the pressure is found by solving the Poisson equation, and the full RK stage velocities are obtained by correcting the intermediate velocities with the updated pressure. This system is solved three consecutive times to obtain full time-step velocities.

To satisfy global mass conservation, an influence-matrix method is employed and is described in some detail by Streett and Hussaini (1991), Danabasoglu, Biringen, and Streett (1990, 1991), and Joslin, Streett, and Chang (1992). For boundary-layer flow, four Poisson-Dirichlet problems are solved for the discrete mode that corresponds to the zero eigenvalue of the system; single Poisson-Neumann problems are solved for all other modes.

The buffer-domain technique introduced by Streett and Macaraeg (1989) is used for the outflow condition. As shown by Joslin, Streett, and Chang (1992) for the flat-plate boundary-layer problem, a buffer length of three disturbance wavelengths is adequate for traveling waves. The disturbances are assumed to be from the discrete spectrum, which exponentially decay with distance from the wall. Both at the wall and in the far field, homogeneous Dirichlet conditions are imposed. The base flow is used for the inflow boundary condition.

Finally, disturbances are forced as unsteady inflow conditions or by unsteady suction and blowing of the wall-normal velocity component through the wall. For the former forcing, u and v profiles that are normalized by u_{max} are generated by some theory (e.g., quasi-parallel linear stability theory), and an amplitude is imposed. For the later forcing, a harmonic source is introduced, the amplitude is based on the wall-normal velocity, and the wave profiles develop naturally in the flow. A similar technique has been used by (among others) Danabasoglu, Biringen, and Streett (1991) in their study of flow control by suction and blowing in a channel flow. Although the disturbances may be generated by random frequency input, the disturbances of interest here are forced with known frequencies. Essentially, this disturbance generator is an alteration to the no-slip boundary conditions, which are conventionally used for the wall condition in a viscous flow problem.

4.3. Linear Stability of Swept Hiemenz Flow

An assessment is made in regard to the value of the Orr-Sommerfeld–Squire equations (OS) formulation in attachment-line flow. Note that OS involves a quasi-parallel flow assumption (i.e., $V = 0$) and that no amplitude information is included in the theory. Figure 4.1 shows the neutral curves predicted with both the OS solver and the linear theory of Hall, Malik, and Poll (1984), which accounts for all linear terms (i.e., nonparallel theory). The nonparallel theory allows for a developing boundary layer (i.e., $V \neq 0$). The largest disagreement in these results appears near the critical-point region. Although accurate growth rates of disturbances may not be obtained with OS as a result of the quasi-parallel constraint, a good estimate of disturbance wavelengths can be obtained. For example, with $R = 800$ and $\omega = 0.1271$, Hall, Malik, and Poll (1984) listed the wave

number $\alpha_r = 0.3385$. According to OS for the same Reynolds number and frequency, the wave number $\alpha_r = 0.3382$ is obtained. Therefore, the terms that are neglected in the governing OS equations, but retained in the Hall, Malik, and Poll (1984) theory, primarily affect the growth and decay rates of the instabilities. Obviously, the spatial growth of the disturbances are of primary importance in transition studies; however, the OS tool can be used to quickly generate base disturbance quantities such as $\alpha_r = f(R,\omega)$ and profiles. These quantities can be used, for example, to determine the initial states for simulations. Although beyond the scope of the present study, this comparison indicates the accuracy of OS in predicting attachment-line instabilities and demonstrates how the nonparallel theory of Hall, Malik, and Poll (1984) improved upon conventional OS.

Figure 4.1 and table 4.1 show the locations on the Reynolds number–frequency plane where the DNS is used to study the linear and nonlinear instabilities for the attachment-line flow. The simulations are performed on

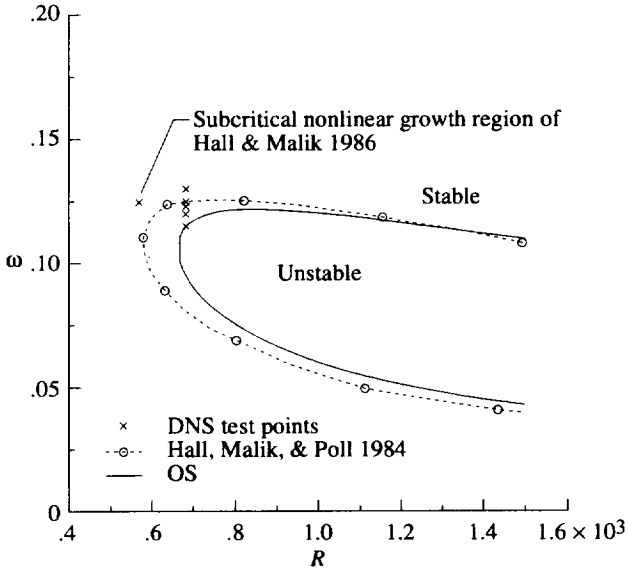

Figure 4.1. Neutral curves, region of subcritical disturbance growth, and computation test points for DNS in attachment-line boundary layer.

Table 4.1. Computational Test Points for DNS

R	ω
570	0.1249
684.2	0.1150
684.2	0.1200
684.2	0.1230
684.2	0.1249
684.2	0.1300

a grid of 661 points (≈60 points per wavelength) along the attachment line and 81 points in the wall-normal direction. The far-field boundary is located at 50δ from the wall, and the computational length along the attachment line is 216.56δ. This attachment-line length corresponds to 11 wavelengths for $R = 570$ and $\omega = 0.1249$. For the time-marching scheme, the disturbance wavelength was divided into 320 time steps per period for small-amplitude disturbances and into 2560 time steps for large-amplitude disturbances (stability considerations). The total Cray Y-MP computer time for a simulation with a single processor was 1.5 hr for small-amplitude disturbances and 12.0 hr for large-amplitude disturbances.

Disturbances for the first simulations are forced at the computational inflow with an amplitude of $A = 0.001$ percent (i.e., arbitrary small amplitude). A Reynolds number R of 570 and a frequency ω of 0.1249 correspond to the region of subcritical growth found by Hall and Malik (1986), where disturbances are linearly stable. Disturbances that evolve in both a base flow that complements the quasi-parallel OS assumptions ($V = 0$) and the full, swept Hiemenz flow are computed with DNS. Figure 4.2 shows the computed disturbance decay rate and the wavelength in the quasi-parallel flow agree exactly with OS. The disturbance that propagates in the complete swept Hiemenz flow closely retains the wavelength predicted by OS but decays at a slower rate than that predicted by OS. This change in decay rate is consistent with the theory of Hall, Malik, and Poll (1984). From this comparison, we find that the wall-normal velocity V terms in the stability equations have a destabilizing effect on the disturbance, which results in the modified neutral curve shown in figure 4.1. This destabilizing influence of the wall-normal linear terms for attachment-line boundary layers is consistent with previous studies on flat-plate Blasius flow. (See El-Hady and Nayfeh 1978; Gaster 1974.)

4.4. Neutral-Curve Region

Additional simulations were conducted in the regions near branches I and II and in the critical Reynolds number region to confirm the neutral curve predicted by the theory. In the region near branch II, the disturbances were forced by suction and blowing at the wall with an amplitude A of 0.001 percent and $R = 684.2$. The growth and decay of various frequency waves are compared with the neutral solution in figure 4.3. The results are in agreement with the neutral curve predicted theoretically by Hall, Malik, and Poll (1984), computed by Spalart (1989), and computed more recently by Jiménez et al. (1990) and Theofilis (1993a, 1993b). This suggests that the chordwise strain contribution, which

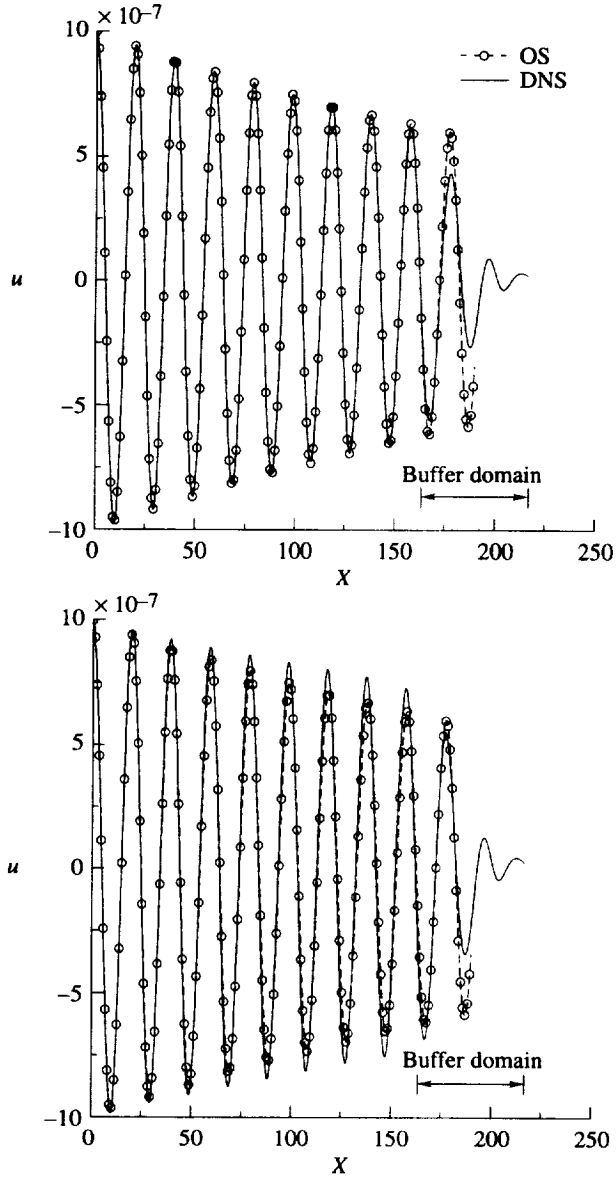

Figure 4.2. Simulated two-dimensional disturbance evolution in parallel ($V = 0$) and nonparallel attachment-line basic flows for $R = 570$ and $\omega = 0.1249$. Samples at $Y = 0.86$.

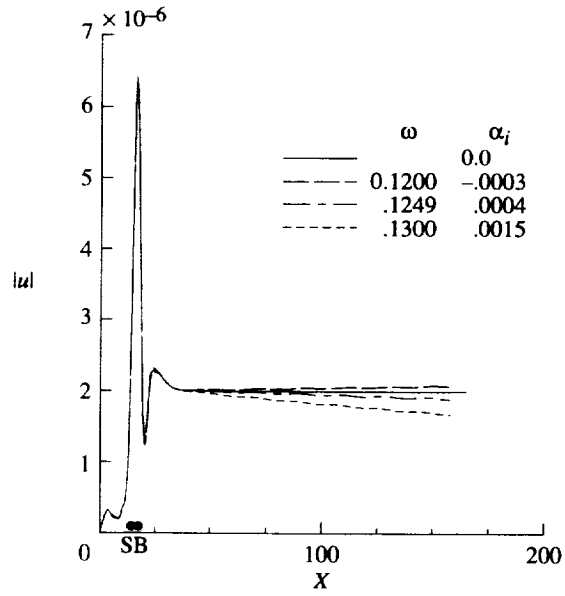

Figure 4.3. Simulated two-dimensional disturbance amplitudes near neutral curve of attachment-line boundary layer at $R = 684.2$.

Table 4.2. Stable or Unstable Regions for Test Points of Table 4.1

R	ω	Region
570	0.1249	Stable
684.2	0.1150	Unstable
684.2	0.1200	Unstable
684.2	0.1230	Stable
684.2	0.1249	Stable
684.2	0.1300	Stable

was neglected from the 2D DNS solver is insignificant for linear computations near the neutral curve.

From the simulation results of 2D small-amplitude disturbances at the test points listed in table 4.1, the resulting stability or instability of those regions are summarized in table 4.2.

4.5. Nonlinear Growth of Subcritical Disturbances

Although the theoretical and computational results agree for the growth and decay properties of linear disturbances along the attachment line, the nonlinear results differ in the subcritical behavior of disturbances. To resolve this discrepancy, the computed results from the present study are compared with the previous studies of Hall and Malik (1986), Jiménez et al. (1990), and Theofilis (1993b). In addition, the effects of suction on unstable modes are documented.

Figure 4.4 shows the evolution of the fundamental wave, the mean-flow distortion, and the harmonics from a simulation forced at the inflow with a large amplitude A of 12 percent for $R = 570$ and $\omega = 0.1249$. After a transient region of adjustment, the fundamental wave encounters subcritical growth, which is in agreement with the weakly nonlinear theory. Contours of instantaneous streamwise ($U + u$) and wall-normal ($V + v$) velocities are shown in figure 4.5. Because the disturbance amplitude is sufficiently large, notable distortions in the base flow are observed as a result of the unsteady disturbance forcing. Figure 4.5 clearly shows a wavelike flow structure in the attachment-line direction. For this flow, instantaneous and mean streamwise and wall-normal

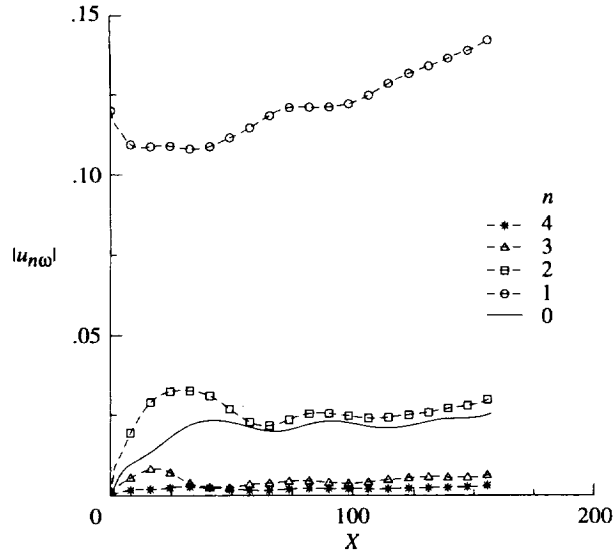

Figure 4.4. Nonlinear subcritical disturbance growth in attachment-line boundary layer at $R = 570$ and $\omega = 0.1249$.

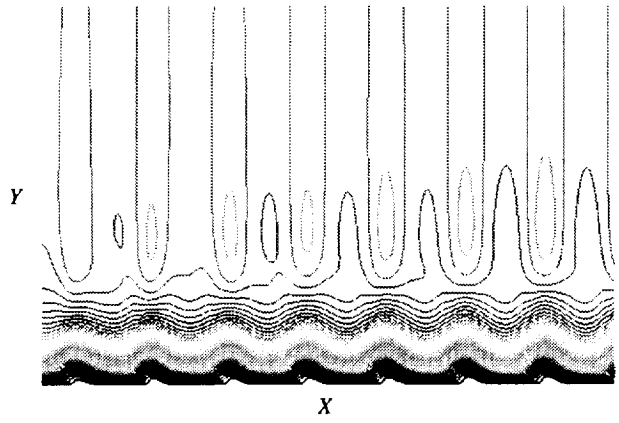

Streamwise $U + u$

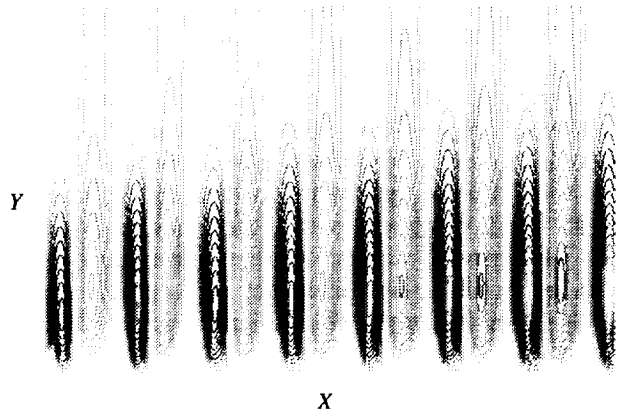

Wall-normal $V + v$

Figure 4.5. Contours of streamwise U and wall-normal V velocities for subcritically growing disturbance in attachment-line boundary layer at $R = 570$ and $\omega = 0.1249$.

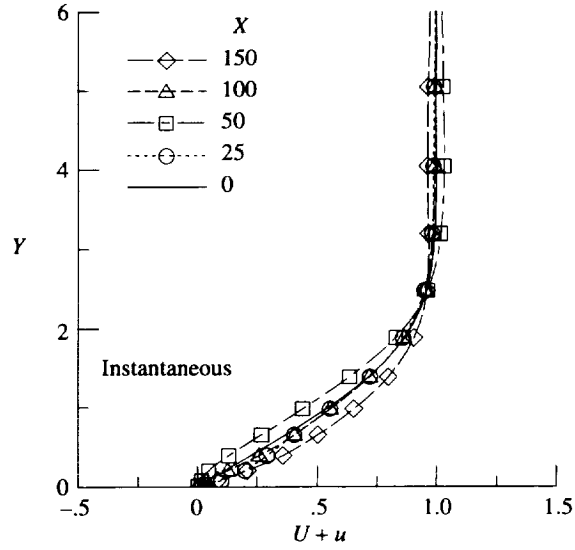

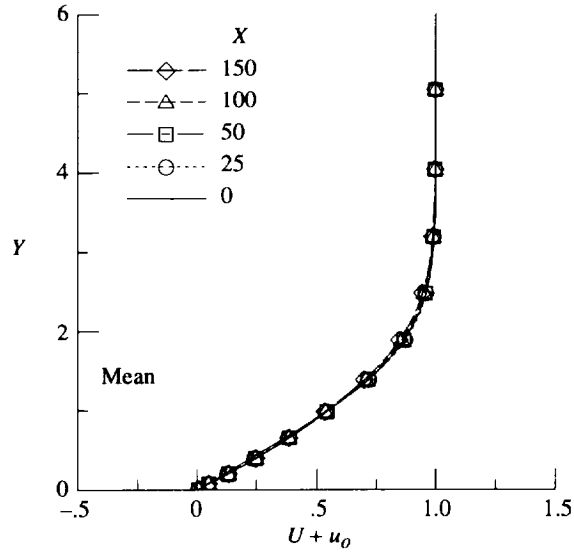

Figure 4.6. Streamwise velocity profiles of nonlinear, subcritically growing disturbance in attachment-line boundary layer at $R = 570$ and $\omega = 0.1249$.

velocity profiles at various attachment-line locations are shown in figures 4.6 and 4.7, respectively. The results in figure 4.6 indicate that spatially varying distortions at fixed time to the base flow are observed, but the mean flow ($U + u_o$), which consists of the base flow and the mean-flow distortion components, shows no noticeable deviation from the base-flow solution. However, the results in figure 4.7 indicate that both the spatially varying and mean wall-normal profiles undergo distortions because of the disturbance. To help understand what effect these mean distortions would have on linear stability calculations, figure 4.8 shows the wall-normal component of the base flow that corresponds to $R = 570$ and

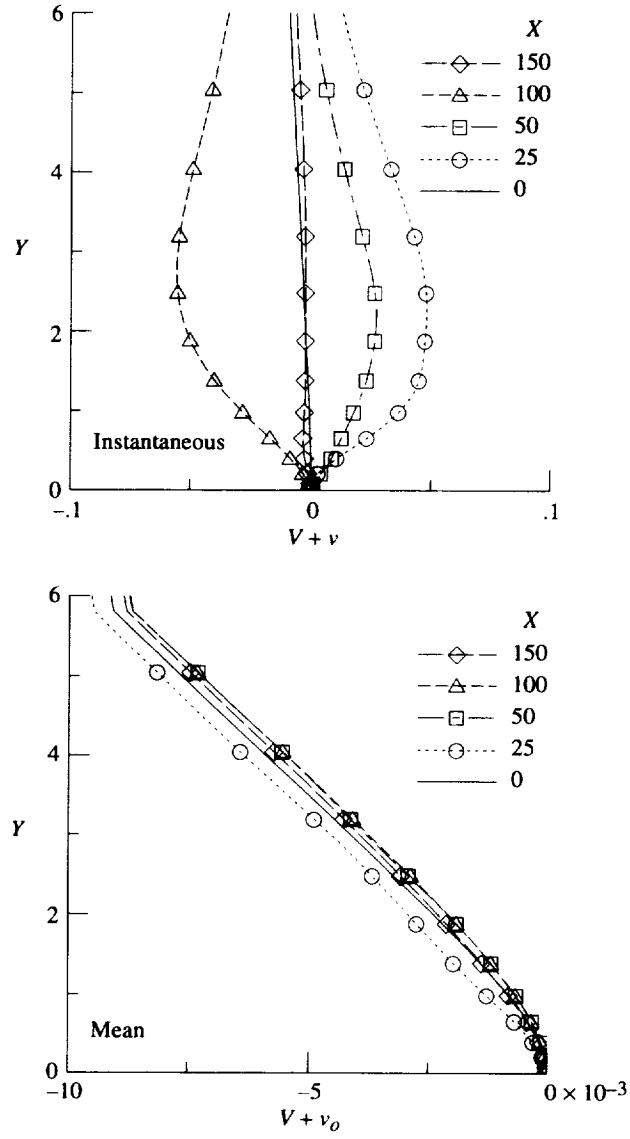

Figure 4.7. Wall-normal velocity profiles of nonlinear, subcritically growing disturbance in attachment-line boundary layer at $R = 570$ and $\omega = 0.1249$.

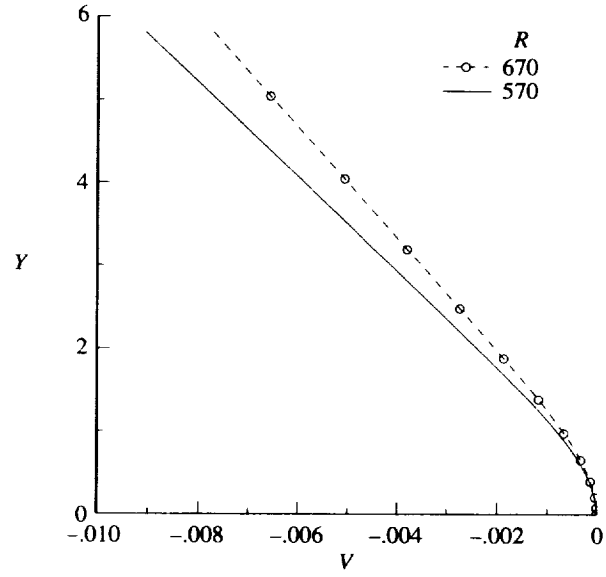

Figure 4.8. Wall-normal component of base flows corresponding to $R = 570$ and 670.

670. A comparison of these base-flow profiles with the mean flow of figure 4.7 shows that a large-amplitude disturbance produces a distortion to the base flow, which causes an effective increase in the base Reynolds number. Evidently, a shift in Reynolds number alone does not account for the growing mode (based on linear stability analysis with the same frequency).

To determine if nonlinear disturbance growth can be found above branch II of the neutral stability curve and to ensure that the subcritical growth obtained both by Hall and Malik (1986) and by DNS shown in figure 4.4 did not artificially result from the disturbance forcing at the inflow boundary, the next sequence of simulations is forced by suction and blowing at decaying modes that correspond to $R = 684.2$ and $\omega = 0.1249$ and are repeated at $R = 684.2$ and $\omega = 0.1230$ (closer to branch II of the neutral curve). For the later test point, the initial amplitudes of the disturbances for each simulation were incrementally increased. The resulting disturbance evolutions are shown in figures 4.9 and 4.10 (normalized by the initial amplitude to show the relative growth effects). The otherwise linearly decaying mode becomes amplified because of the nonlinear forcing. Interestingly, as the initial amplitude is increased, the fundamental wave receives a smaller percentage of the total energy injected into the flow because other modes receive a larger percentage of the energy.

Finally, the nonlinear simulation results of large-amplitude initial disturbances broaden the neutral curve toward higher frequencies and lower critical Reynolds numbers, similar to the influence of nonparallel effects on linear disturbance growth. This postulation is sketched in figure 4.11, where the nonlinear-influence curve is artificial and serves to show how the now "neutral curve" might shift to reflect that certain nonlinear modes are growing while others are decaying. Note, that this influence of single nonlinear disturbance growth does not resolve the discrepancy in Reynolds number between linear growth (table 2.1) and bypass (table 2.2) regions.

At this point it is not clear why the results of Jiménez et al. (1990) do not agree with either the present DNS results or the previous theory and computations of Hall and Malik (1986); however, from the present initial amplitudes required to achieve this subcritical growth,

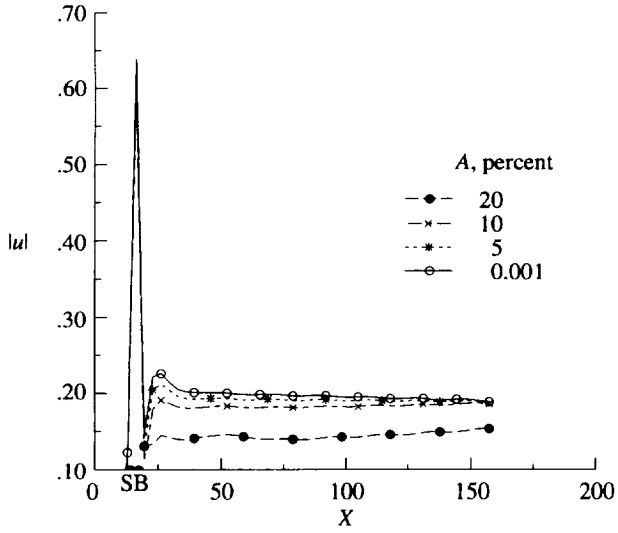

Figure 4.9. Nonlinear disturbance growth in attachment-line boundary layer at R = 684.2 and ω = 0.1249. Disturbances normalized by initial amplitudes.

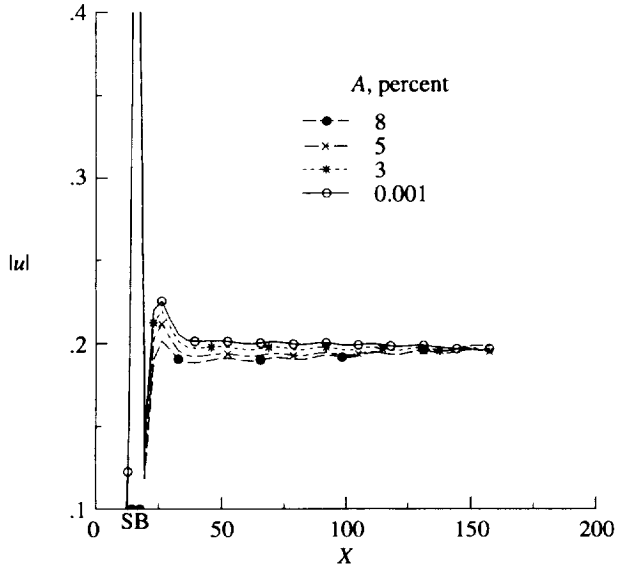

Figure 4.10. Nonlinear disturbance growth in attachment-line boundary layer at R = 684.2 and ω = 0.1230. Disturbances normalized by initial amplitudes.

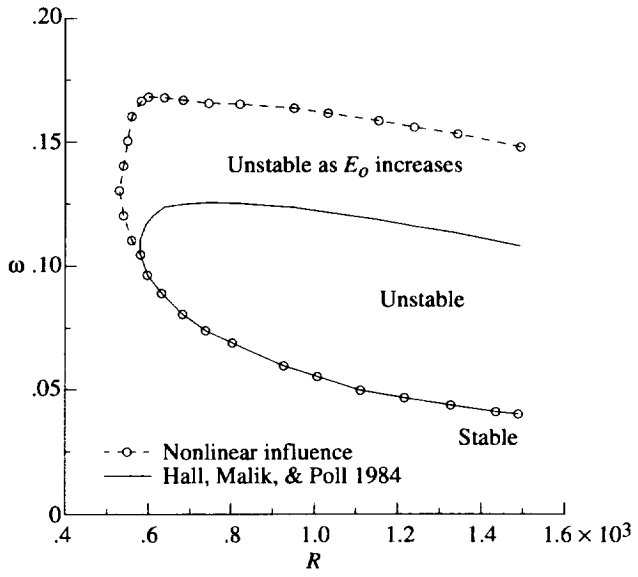

Figure 4.11. Impact of large-amplitude disturbances on region of disturbance growth.

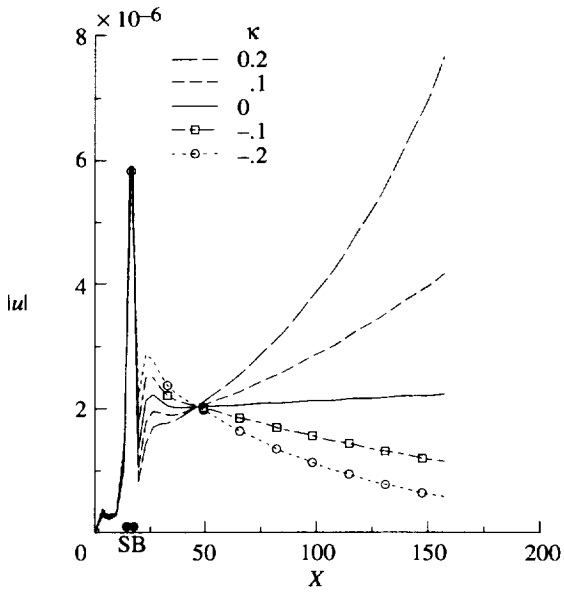

Figure 4.12. Control of linear disturbance growth in attachment-line boundary layer at R = 684.2 and ω = 0.1150 with suction.

Theofilis (1993b) apparently could not force a disturbance with sufficient amplitude to realize this nonlinear growth.

4.6. Effect of Suction and Blowing on Disturbance

Finally, the effect of both steady suction and steady blowing on linear and nonlinear disturbance growth is documented. The amplification of linear disturbances influenced by suction and blowing is shown in figure 4.12 for R = 684.2 and ω = 0.1150. The results indicate that suction stabilizes the disturbance and blowing significantly destabilizes the disturbance. The effects of suction and blowing on disturbances computed by DNS are in agreement with the theory of Hall, Malik, and Poll (1984) for small-amplitude disturbances.

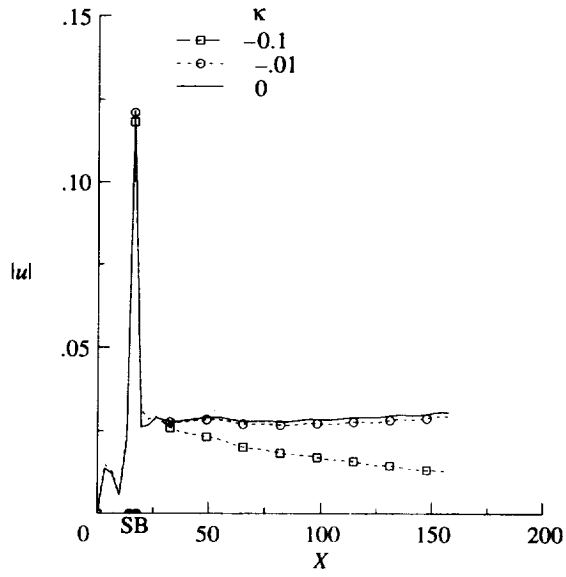

Figure 4.13. Control of nonlinear disturbance growth in attachment-line boundary layer at R = 684.2 and ω = 0.1249 with suction.

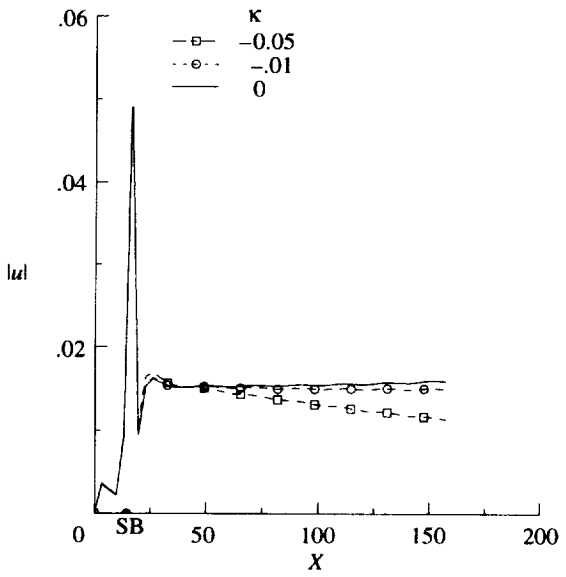

Figure 4.14. Control of nonlinear disturbance growth in attachment-line boundary layer at R = 684.2 and ω = 0.1230 with suction.

For the nonlinear subcritical case near branch II, the effects of steady suction on the disturbance amplitude are shown in figures 4.13 and 4.14 for the largest amplitude disturbances of figures 4.9 and 4.10. The results further demonstrate that small amounts of suction can be used to stabilize disturbances that otherwise nonlinearly grow

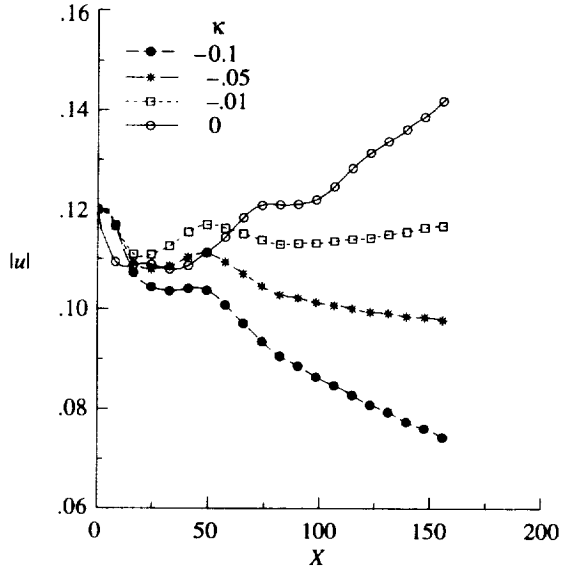

Figure 4.15. Control of nonlinear subcritical disturbance growth in attachment-line boundary layer at R = 570 and ω = 0.1249 with suction.

near branch II of the neutral curve. Larger forcing amplitudes are required to obtain nonlinear growth with Reynolds numbers and frequencies farther away from the neutral curve, and, as expected, larger amounts of suction are required to stabilize these disturbances.

To control the subcritical growth of disturbances, various levels of suction are employed. Although Hall and Malik (1986) noted that suction makes the flow more susceptible to subcritical disturbance growth, figure 4.15 shows that this subcritical disturbance growth shown in figure 4.4 can be controlled by using small levels of suction. If the 2D DNS results mimic the actual 3D behavior of the flow, then large-amplitude disturbances generated on the attachment line can be controlled with a sufficient amount of suction.

5. Attachment-Line Disturbances for Quasi-3D Assumption

In section 4, an alternate disturbance form was used, where the velocity component w of the disturbance and the transverse shear of the mean flow were neglected and the disturbance became 2D along the attachment line. This implied that $w = 0$ and $\partial w/\partial Z = 0$ on the attachment line. Although this simplification was not consistent with the equations of motion, the results of this section (which retain the previously neglected terms) show that results from the 2D assumption yield similar qualitative behavior of the computed disturbances.

5.1. Form of Disturbances

In general, disturbances on and near a 3D attachment-line region are of the 3D nature, requiring solutions of the full 3D Navier-Stokes equations. However, as assumed in the original theoretical study by Hall, Malik, and Poll (1984) and confirmed in the DNS computations by Spalart (1989), a single mode in the attachment-line region of swept Hiemenz flow can take the form

$$\left.\begin{aligned} u &= u(x,y,t) \\ v &= v(x,y,t) \\ w &= w(x,y,t)\times Z \end{aligned}\right\} \tag{5.1}$$

This form permits the velocity component w of the disturbance to have a linear variation with distance from the attachment line, which is the same as the base flow. (See eq. (3.2).) Whereas the amplitude of w varies linearly with distance from the attachment line, the components u and v remain uniform with distance from the attachment line. The subsequent computations by Jiménez et al. (1990) and Theofilis (1993a, 1993b) used this same disturbance form and showed linear results near the neutral curve which were in agreement with the Hall, Malik, and Poll (1984) theory and nonlinear results that failed to achieve the subcritical growth predicted by the weakly nonlinear theoretical and computational results of Hall and Malik (1986).

A final series of simulations is performed with the linear variance form described by equations (5.1) and used by Hall and Malik (1986) for their theory and computations and used in subsequent computations by Jiménez et al. (1990) and Theofilis (1993a, 1993b). This dependence of equations (5.1) requires solutions of the following momentum and continuity equations:

$$\frac{\partial u}{\partial X} + \frac{\partial v}{\partial Y} + w = 0 \tag{5.2}$$

$$\frac{\partial u}{\partial t} + (U+u)\frac{\partial u}{\partial X} + (V+v)\frac{\partial u}{\partial Y} + v\frac{\partial U}{\partial Y} = -\frac{\partial p}{\partial X} + \frac{1}{R}\left(\frac{\partial^2 u}{\partial X^2} + \frac{\partial^2 u}{\partial Y^2}\right) \tag{5.3}$$

$$\frac{\partial v}{\partial t} + (U+u)\frac{\partial v}{\partial X} + (V+v)\frac{\partial v}{\partial Y} + v\frac{\partial V}{\partial Y} = -\frac{\partial p}{\partial Y} + \frac{1}{R}\left(\frac{\partial^2 v}{\partial X^2} + \frac{\partial^2 v}{\partial Y^2}\right) \tag{5.4}$$

$$\frac{\partial w}{\partial t} + (U+u)\frac{\partial w}{\partial X} + (V+v)\frac{\partial w}{\partial Y} + v\frac{\partial W}{\partial Y} + (2W+w)w = -\frac{\partial p}{\partial Z} + \frac{1}{R}\left(\frac{\partial^2 w}{\partial X^2} + \frac{\partial^2 w}{\partial Y^2}\right) \tag{5.5}$$

The results for the disturbance described by equations (5.2)–(5.5), hereafter referred to as "3D disturbances" in the rest of section 5, are shown to qualitatively agree with a 2D solution and the theory of Hall and Malik (1986) provided the disturbance pressure gradient is of a particular form in the flow-acceleration direction.

5.2. Numerical Methods of Solution

The numerical procedure as described in section 4.2 is used for the present system of equations. The disturbances are forced as unsteady inflow conditions. The profiles u and v that are normalized by u are generated by some theory (e.g., quasi-parallel linear stability theory), and an amplitude is imposed.

5.3. 3D Nonlinear Subcritical Disturbances

Note that the results in section 4.4 are achieved through the 2D simplification. In this section, the 3D instabilities are determined by solving equations (5.2)–(5.5). Note, that by using the disturbance form given in equations (5.1), the Z dependence of the disturbance is removed from the theoretical-computational problem, except for a partial derivative of the pressure in equation (5.4). In fact, it is from this observation that we find a difference between the studies of Hall and Malik (1986) and Jiménez et al. (1990). It is apparent from the manuscripts that different assumptions were made for the pressure behavior in the flow-acceleration direction.

In the studies of Hall, Malik, and Poll (1984) and Hall and Malik (1986), the disturbance pressure was a function of (X,Y) only; this leads to

$$\frac{\partial p}{\partial Z} = 0\times Z \tag{5.6}$$

in equation (5.4). With this pressure form, a series of simulations was conducted by solving equations (5.2)–(5.5). Figure 5.1 shows the fundamental mode and first harmonic of the attachment-line direction velocity component compared with the previous 2D mode (fig. 4.2). In agreement with the 2D qualitative behavior, the 3D mode undergoes subcritical growth. Quantitative differences are apparent and expected due to the addition of equation (5.4) and the modified continuity equation. The energy content with distance along the attachment line is probably a better measure of total disturbance growth or decay. Figure 5.2 shows this disturbance energy for various subcritical Reynolds numbers. For a fixed initial

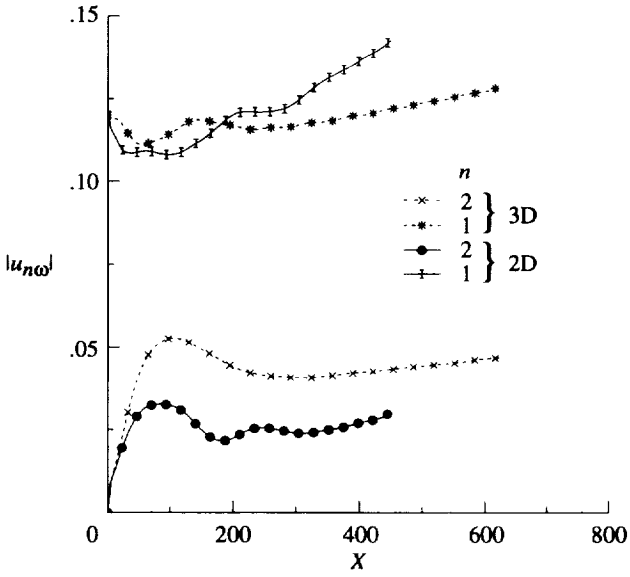

Figure 5.1. Nonlinear subcritical growth of 2D and 3D disturbances in attachment-line boundary layer at R = 570 and $\omega = 0.1249$.

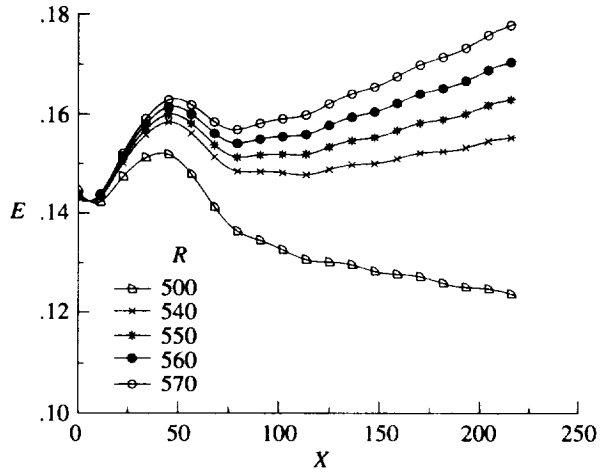

Figure 5.2. Nonlinear subcritical energy of 3D disturbances in attachment-line boundary layer with Reynolds number at $\omega = 0.1249$.

disturbance amplitude, it is clear that the disturbance energy increases with distance along the attachment line, in agreement with the theory and computations of Hall and Malik (1986) and with the earlier 2D modal approximation. These results support the conjecture shown in figure 4.11; namely, for a fixed large initial amplitude, there are distinct regions of disturbance growth and decay which can be described by "neutral curves."

In the study of Jiménez et al. (1990), the disturbance pressure was assumed to be of the same form as that of

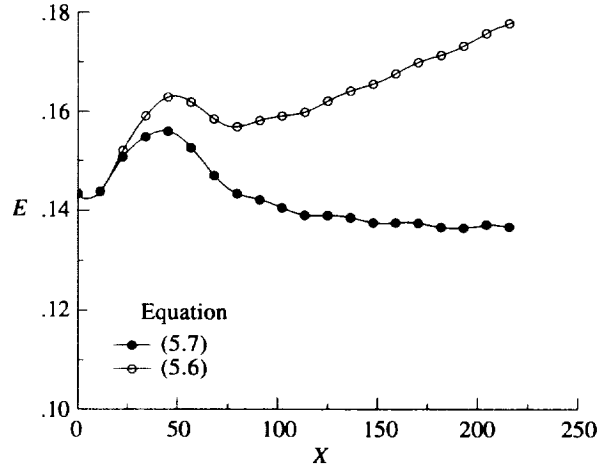

Figure 5.3. Nonlinear subcritical energy of 3D disturbances in attachment-line boundary layer at R = 570 and $\omega = 0.1249$.

the base flow. Namely, pressure varied with the square of distance from the attachment line in the flow-acceleration direction. They arrived at a pressure gradient in the flow-acceleration direction which took the form

$$\frac{\partial p}{\partial Z} = -1 \times Z \tag{5.7}$$

Using this pressure form, a final simulation was conducted and the results are presented in figure 5.3 with the results from equation (5.6) as the flow-acceleration pressure gradient. This simple difference in pressure leads to a decaying mode instead of nonlinear subcritical growth. Hence, the discrepancy between the Jiménez et al. (1990) computations and the computations and weakly nonlinear theory of Hall and Malik (1986) lie with an effective pressure source difference.

This discrepancy presented in figure 5.3 leads to an additional puzzling question: Which pressure form should be used for future simulations? The correct pressure form for the disturbances studied by Hall and Malik (1986) and Jiménez et al. (1990) is demonstrated in section 6 by looking at the pressure solution of a fully 3D simulation.

6. Attachment-Line Disturbances for Full 3D Modes

6.1. Form of Disturbances

In this section, the disturbances are forcibly imposed into the boundary layer by unsteady suction and blowing with the wall-normal velocity component through the wall (harmonic-source generators). An equal amount of mass injected by blowing is extracted by suction so that

zero net mass is added to the boundary layer. A similar technique has been used by (among others) Danabasoglu, Biringen, and Street (1991) in their study of periodic control by suction and blowing. Although the disturbances may be generated by random frequency input, the disturbances of interest here are forced with known frequencies. Essentially, this disturbance generator is an alteration to the no-slip boundary conditions which are conventionally used for the wall condition in a viscous flow problem.

6.2. Numerical Methods of Solution

In the attachment-line (X) direction, fourth-order central finite differences are used for the pressure equation and sixth-order compact differences are used for the momentum equations in the interior of the computational domain. At the boundary and near-boundary nodes, fourth-order forward and backward differences are used. The discretization yields a pentadiagonal system for the finite-difference scheme and a tridiagonal system for the compact-difference scheme. The approximations can be solved efficiently by appropriate backward and forward substitutions.

In both the wall-normal (Y) and flow-acceleration (Z) directions, the Chebyshev series is used to approximate the disturbances at Gauss-Lobatto collocation points. In particular, the use of the Chebyshev series enables an efficient pressure solver. Because this series and its associated spectral operators are defined on $[-1,1]$ and the physical problem of interest has a truncated domain $[0,Y_{max}]$ and $[-Z_{max},Z_{max}]$, transformations are employed. Furthermore, stretching functions are used to cluster the grid near both the wall and the attachment line.

The same time-marching scheme and inflow and outflow boundary conditions as described in section 4.2 are used in the 3D DNS code.

To efficiently solve the resulting Poisson problem, the tensor-product method of Lynch, Rice, and Thomas (1964) is used. The discretized form of the Poisson equation for the pressure is

$$(\mathbf{L}_x \otimes \mathbf{I} \otimes \mathbf{I} + \mathbf{I} \otimes \mathbf{L}_y \otimes \mathbf{I} + \mathbf{I} \otimes \mathbf{I} \otimes \mathbf{L}_z)p = \overline{RHS} \quad (6.1)$$

where p is the desired pressure solution; the right side of the equation $\overline{RHS}$ results from the time-splitting procedure; $\mathbf{I}$ is the identity matrix; $\mathbf{L}_x$ is the attachment-line-directed central finite-difference operator; $\mathbf{L}_y$ and $\mathbf{L}_z$ are the wall-normal-directed and flow-acceleration-directed spectral operators; and $\otimes$ denotes a tensor product. By decomposing the operators $\mathbf{L}_y$ and $\mathbf{L}_z$ into their respective eigenvalues and eigenvectors, we find

$$\left.\begin{aligned} \mathbf{L}_y &= \mathbf{Q}\Lambda_y\mathbf{Q}^{-1} \\ \mathbf{L}_z &= \mathbf{S}\Lambda_z\mathbf{S}^{-1} \end{aligned}\right\} \quad (6.2)$$

where $\mathbf{Q}$ and $\mathbf{S}$ are the eigenvectors of $\mathbf{L}_y$ and $\mathbf{L}_z$, $\mathbf{Q}^{-1}$ and $\mathbf{S}^{-1}$ are inverse matrices of $\mathbf{Q}$ and $\mathbf{S}$, and Λ_y and Λ_z are the eigenvalues of $\mathbf{L}_y$ and $\mathbf{L}_z$. The solution procedure reduces to the following sequence of operations to determine the pressure p:

$$\left.\begin{aligned} p^* &= (\mathbf{I} \otimes \mathbf{Q}^{-1} \otimes \mathbf{S}^{-1})\overline{RHS} \\ p^\dagger &= (\mathbf{L}_x \otimes \mathbf{I} \otimes \mathbf{I} + \mathbf{I} \otimes \Lambda_y \otimes \mathbf{I} + \mathbf{I} \otimes \mathbf{I} \otimes \Lambda_z)^{-1} p^* \\ p &= (\mathbf{I} \oplus \mathbf{Q} \otimes \mathbf{S})p^\dagger \end{aligned}\right\} \quad (6.3)$$

Because the number of grid points in the attachment-line direction is typically an order of magnitude larger than the wall-normal and flow-acceleration directions, the operator $\mathbf{L}_x$ is much larger than both $\mathbf{L}_y$ and $\mathbf{L}_z$. Because $\mathbf{L}_x$ is large and has a sparse pentadiagonal structure and because Λ_y and Λ_z influence the diagonal only, an LU decomposition is performed for the second stage of equations (6.3) once, and forward and backward solves are performed for each time step of the simulation. The first and third steps of the pressure solver in equations (6.3) involve matrix multiplications.

To obtain the attachment-line-directed operator $\mathbf{L}_x$, central finite differences are used. To find the wall-normal $\mathbf{L}_y$ and flow-acceleration $\mathbf{L}_z$ operators, the following matrix operations are required:

$$\left.\begin{aligned} \mathbf{L}_y &= \mathbf{I}_{GL}^{G}\mathbf{D}_y\tilde{\mathbf{D}}_y\mathbf{I}_{G}^{GL} \\ \mathbf{L}_z &= \mathbf{I}_{GL}^{G}\mathbf{D}_z\tilde{\mathbf{D}}_z\mathbf{I}_{G}^{GL} \end{aligned}\right\} \quad (6.4)$$

where $\mathbf{D}_y$ is a spectral wall-normal derivative operator for the stretched grid, $\mathbf{D}_z$ is the spectral derivative operator that is grid clustered in the attachment-line region, and $\tilde{\mathbf{D}}_y$ and $\tilde{\mathbf{D}}_z$ are the derivative operators with the first and last rows set to 0. The interpolation matrix $\mathbf{I}_{GL}^{G}$ operates on variables at Gauss-Lobatto points and transforms them to Gauss points; the interpolation matrix $\mathbf{I}_{G}^{GL}$ performs the inverse operation. The spectral operators are described in detail by Canuto et al. (1988) and Joslin, Street, and Chang (1993).

The operators $\{\mathbf{L}_x,\mathbf{L}_y,\mathbf{L}_z\}$, the eigenvalue matrices $\{\Lambda_y,\Lambda_z\}$, the eigenvector matrices $\{\mathbf{Q},\mathbf{Q}^{-1},\mathbf{S},\mathbf{S}^{-1}\}$, and the influence matrix are all mesh-dependent matrices

and must be calculated only once. The wall-normal direction spectral operators and $\overline{RHS}$ are given in Joslin, Street, and Chang (1993); the same form is used for the flow-acceleration direction.

Both at the wall and in the far field, homogeneous Dirichlet conditions are imposed. Homogeneous Dirichlet and Neumann conditions have been used in the flow-accelerated direction. With either condition, the disturbance will develop in the same manner along the attachment line, provided that the boundaries are sufficiently far from the attachment-line region. The base flow is used for the inflow boundary condition.

6.3. Quasi-2D Symmetric Disturbances

The spatial evolution of three-dimensional disturbances is computed by direct numerical simulation, which involves the solution to the unsteady, nonlinear, three-dimensional Navier-Stokes equations. The simulations are performed on a grid of 661 points (≈60 points per wavelength) along the attachment line, 81 points in the wall-normal direction, and 25 points in the flow-acceleration direction. The far-field boundary is located at 50δ from the wall, the computational length along the attachment line is 216.56δ, and the flow-acceleration boundaries are located $\pm 100\delta$ from the attachment line. For the time-marching scheme, the disturbance wavelength was divided into 320 time steps per period. The total Cray Y-MP computer time for a simulation with a single processor was approximately 25 hr. As shown in figure 6.1, the parameter regions of interest consist of a region of linear disturbance growth, a region of linear disturbance decay (which is the region of nonlinear, subcritical disturbance growth identified by Hall and Malik (1986)), the upper and lower branches of the neutral curve, and the critical region predicted by the nonparallel theory of Hall, Malik, and Poll (1984).

This study begins by validating the simulation results for infinitesimal disturbances with hydrodynamic stability theory with the special case of a frozen base flow. Nonparallel terms (i.e., the wall-normal base flow components) for the equations are included in the simulation, and the instabilities are compared with the frozen-flow disturbance properties. Next, aspects of disturbance development on and near the attachment line are compared for quasi-two-dimensional and point-source harmonic source generators with the theory of Hall, Malik, and Poll (1984). The effects of suction on the instabilities are documented. Conclusions are drawn and the importance of this study on the global problem of attachment-line instability is ascertained. Finally, future directions for continuing the study of the problem of instabilities in attachment-line boundary layers are suggested.

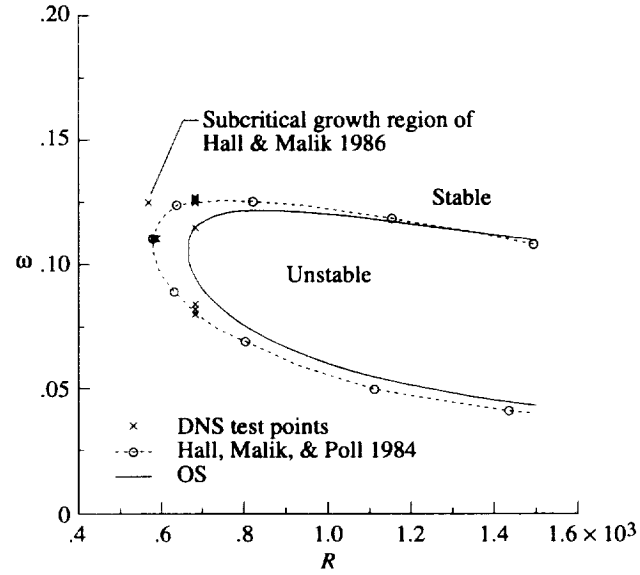

Figure 6.1. Neutral curves, region of subcritical disturbance growth, and computational test points for DNS in attachment-line boundary layer.

The nonparallel theory of Hall, Malik, and Poll (1984) outlined the stable and unstable regions for infinitesimal disturbances. In a segment of the subcritical region, large-amplitude disturbances were found by Hall and Malik (1986) to exhibit nonlinear amplification. The results for two-dimensional, spatial direct numerical simulation in section 4 confirmed this subcritical growth phenomenon. In this section, $R = 570$ and $\omega = 0.1249$, parameters in the subcritical region, are used in the study of the evolution of small-amplitude three-dimensional disturbances. The results are compared with linear stability theory and previous two-dimensional results.

To compare with the two-dimensional theory and previous simulations, a quasi-two-dimensional disturbance is initiated in the three-dimensional flow. At best, this disturbance is an approximation to a true two-dimensional disturbance mode. To generate this two-dimensional disturbance, a harmonic source is used that is elongated ($-44.2 < Z < 44.2$) in the flow-acceleration direction. This disturbance-forcing method is comparable with using a vibrating ribbon to generate two-dimensional disturbances for wind-tunnel experiments. The qualitative features of a disturbance generated by the harmonic source with a small amplitude (e.g., $A = 0.001$ percent) are shown in figure 6.2. The disturbance evolution is viewed from above and along the attachment line. The wave travels along the attachment line without significant three-dimensional features. However, because the base flow is accelerating away from the attachment line (in the $\pm Z$-directions), wave spreading occurs with

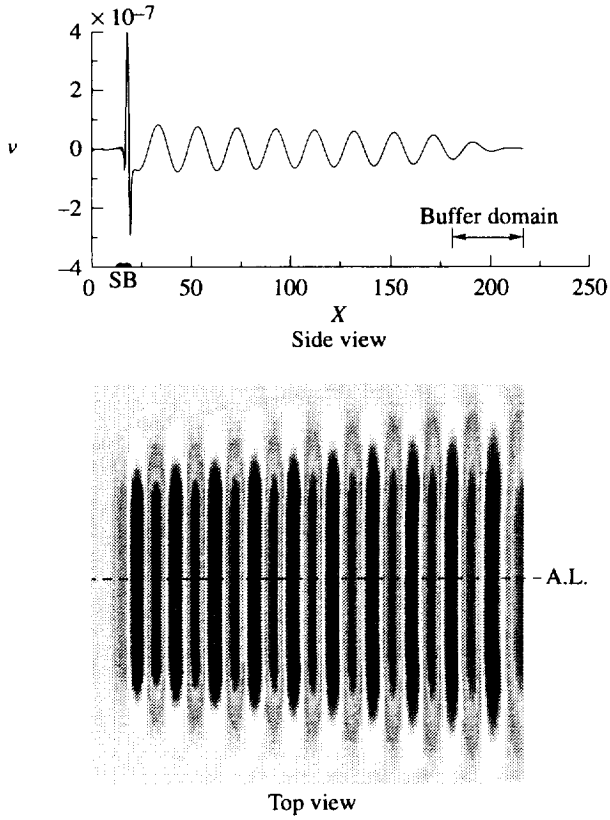

Figure 6.2. Three-dimensional traveling wave in attachment-line boundary layer for $R = 570$ and $\omega = 0.1249$.

distance from the harmonic source, and the rate of spreading increases with distance along the attachment line.

Quasi-two-dimensional simulation results for both a quasi-parallel base flow (i.e., $V = 0$) and the full swept Hiemenz flow are compared with linear stability theory, and the results are shown in figure 6.3. The amplitude, decay rate, and wavelength of disturbances simulated with the quasi-parallel flow are in very good quantitative agreement with the results of two-dimensional linear stability theory. This agreement suggests that in this parameter region the elongated harmonic source can approximate a two-dimensional disturbance along the attachment line. Figure 6.3 also shows that the full swept Hiemenz base flow destabilizes disturbances due to the inclusion of the velocity component V. This destabilizing feature is consistent with the results reported in the two-dimensional nonparallel studies by Hall, Malik, and Poll (1984).

To further demonstrate the two-dimensional nature of the disturbance generated with the elongated harmonic source, figure 6.4 shows the attachment-line results compared with results at distances of 13δ and 35δ off the

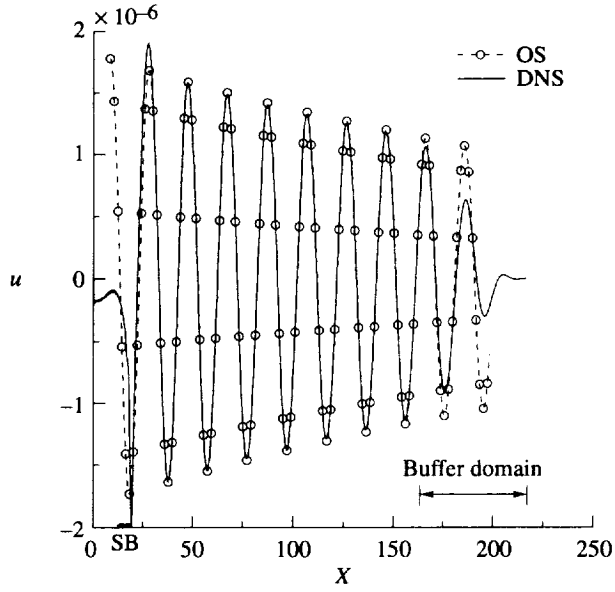

(a) Parallel basic flow approximation. $V = 0$.

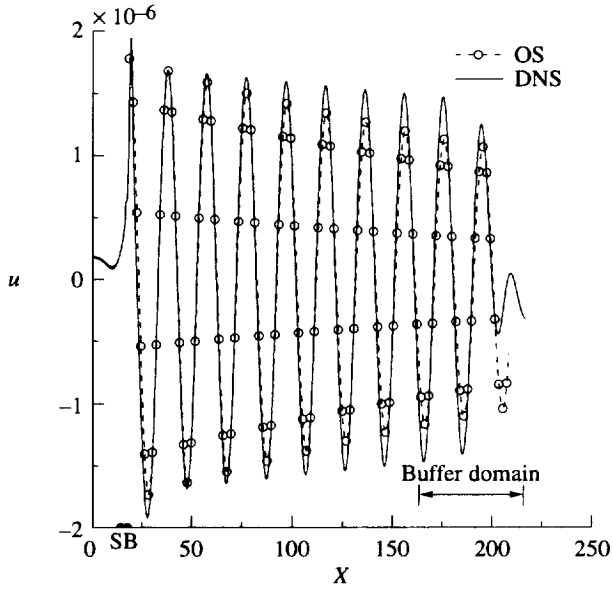

(b) Three-dimensional attachment-line basic flow.

Figure 6.3. Simulated two-dimensional disturbance evolution for $R = 570$ and $\omega = 0.1249$.

attachment line. The evolution patterns are identical out to near 35δ, where small deviations are observed. This observation implies that the elongated harmonic source is generating primarily two-dimensional waves and that the attachment-line velocity component is dominant (i.e., the amplitude of the velocity component w of the disturbance is too small to modify the dominant component u). Figure 6.5 shows velocity profiles for u and w at $Z = 13\delta$ and

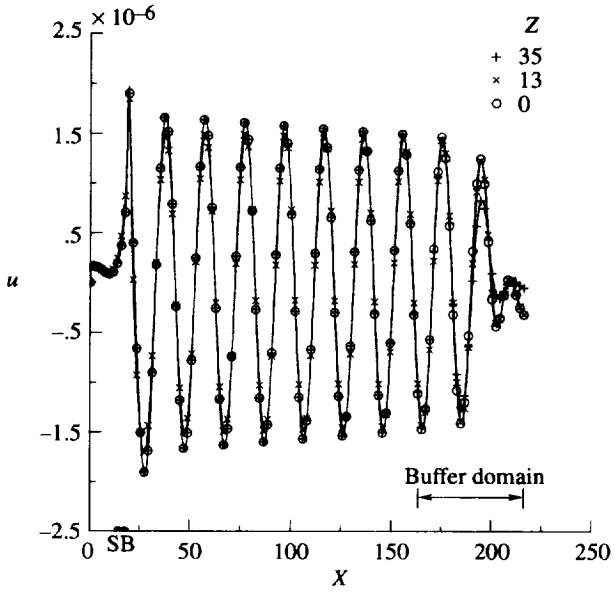

Figure 6.4. Flow-acceleration variation of simulated two-dimensional disturbance evolution in three-dimensional attachment-line basic flow for $R = 570$ and $\omega = 0.1249$.

35δ. Although only small differences are found with velocity components u, the velocity components w are in strong disagreement. This disagreement results from the variation of that component with distance from the attachment line. Note that the velocity w is an order of magnitude smaller than the velocity u; this is the reason for the good agreement between the velocity u on the attachment line with the same components off the attachment line. Furthermore, although no symmetry assumption is made, flow symmetry about the attachment line is realized with this particular harmonic-source generator.

In figures 6.6 and 6.7, three-dimensional simulation results on the attachment line are compared with previous two-dimensional simulation results in section 4.3. Figure 6.6 clearly shows a significant amplitude disparity between the two- and three-dimensional results. Because the three-dimensional simulations contain a flow-acceleration velocity component w, an additional degree of freedom is available to disperse (or absorb) energy. Hence, the harmonic-source generator forces less energy into the attachment-line velocity component u. The normalized two-dimensional and three-dimensional results are also shown in figure 6.6 to enable a growth-rate comparison. The disturbance is slightly more destabilized in the full three-dimensional flow than in the two-dimensional flow approximation. Similar qualitative differences are evident when disturbance growth rates in quasi-parallel flow are compared with those in nonparallel flows. Finally, the disturbance velocity profiles at $X = 100$ are presented in figure 6.7. The shapes of the

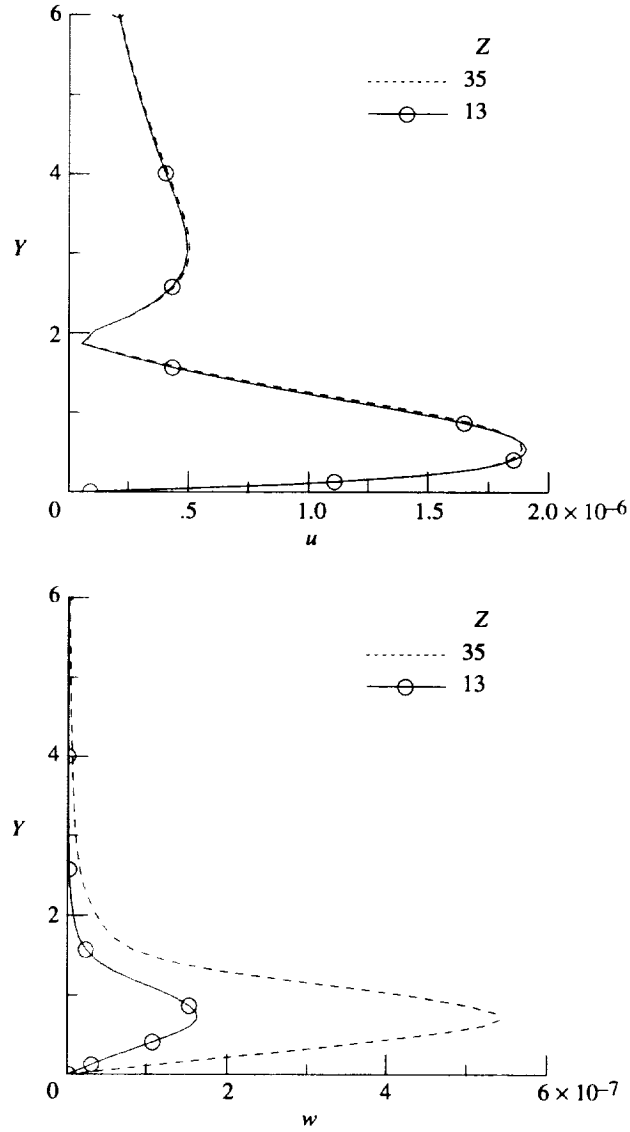

Figure 6.5. Three-dimensional disturbance velocity profiles at $X = 100$ near attachment line for $R = 570$ and $\omega = 0.1249$.

compared profiles agree well. The results demonstrate that two-dimensional simulations capture the qualitative features of the true three-dimensional flow; in addition, because a third degree of freedom (w,z) is not present in the two-dimensional simulations, amplitude information is overpredicted and growth-rate information is underpredicted. These results suggest that much larger disturbances are required to generate subcritical disturbance growth in the three-dimensional flow (if subcritical growth is possible in the three-dimensional flow).

In the nonparallel theory of Hall, Malik, and Poll (1984), the z-dependent form for the flow-accelerated velocity component w was a key assumption, which led to a system of ordinary differential equations rather than

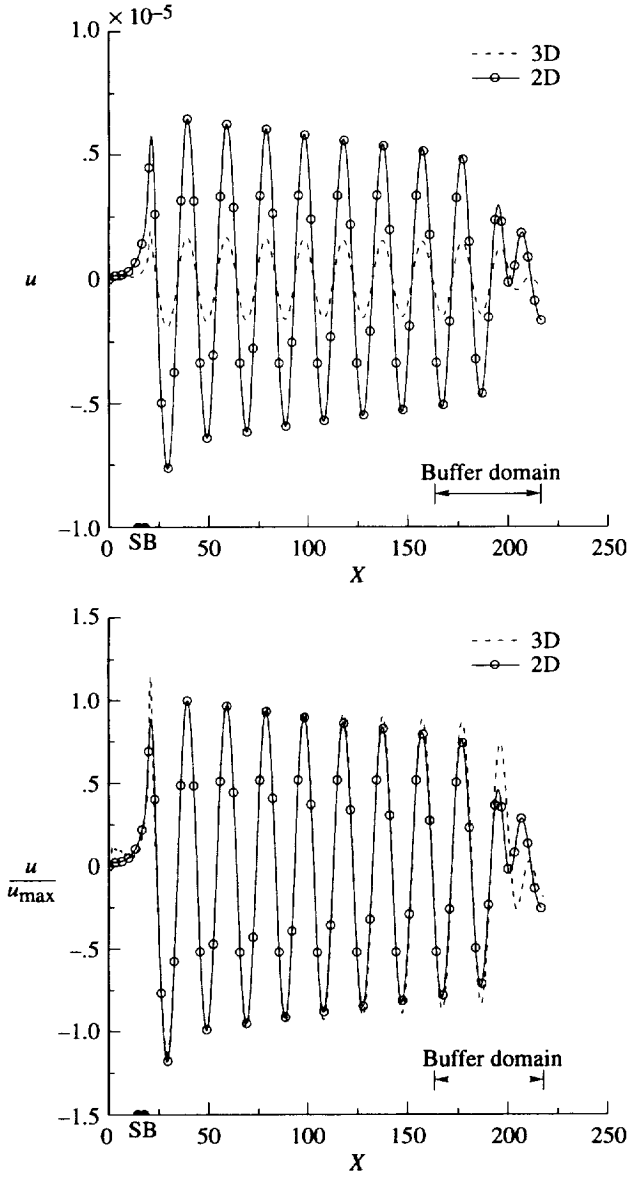

Figure 6.6. Two- and three-dimensional disturbance evolutions in three-dimensional attachment-line boundary layer for $R = 570$ and $\omega = 0.1249$.

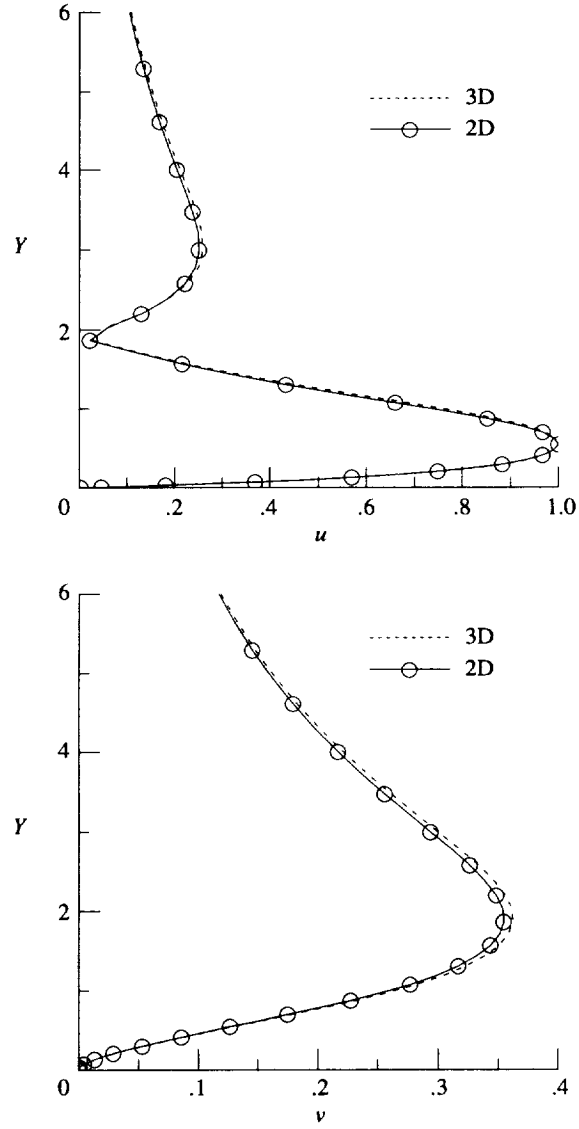

Figure 6.7. Two- and three-dimensional disturbance velocity profiles at $X = 100$ normalized by component u in attachment-line boundary layer for $R = 570$ and $\omega = 0.1249$.

partial differential equations. This assumed form is equivalent to the base-flow form: $W \rightarrow W_o Z$. Figure 6.8 shows the maximum amplitudes of the flow-accelerated velocity component at $X = 100$ and away from the attachment line. For the present harmonic source, this z-dependent disturbance form assumed by Hall, Malik, and Poll (1984) is realized in the simulation near the attachment line; however, because the harmonic source has a finite length, the disturbance behavior near the harmonic-source ends deviates from the expected z dependence. The harmonic-source ends cause a perturbation to the flow that is shown both in figure 6.8 and in a top view of the flow in figure 6.9. Similar difficulties in disturbance initialization can be found in the experiments; however, the core of the test region (i.e., the attachment line) is not significantly contaminated by these end effects.

We address the question in section 5.3 with respect to the pressure forms used by Hall and Malik (1986) and Jiménez et al. (1990) by comparing with the pressure from the present 3D simulation; this comparison will provide confirmation of either subcritical growth or decay. At an arbitrary distance downstream of the source, the pressure is shown in figure 6.10, where the maximum pressure is shown as a function of distance from the

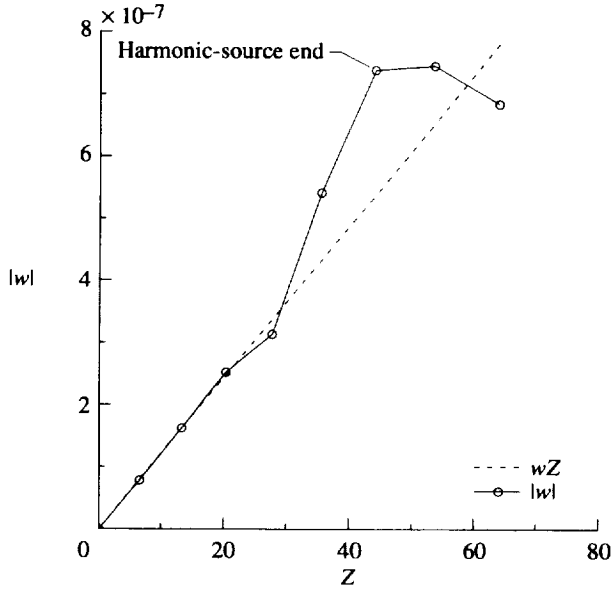

Figure 6.8. Maximum flow-accelerated disturbance velocity w with distance from attachment line at X = 100, R = 570, and $\omega = 0.1249$.

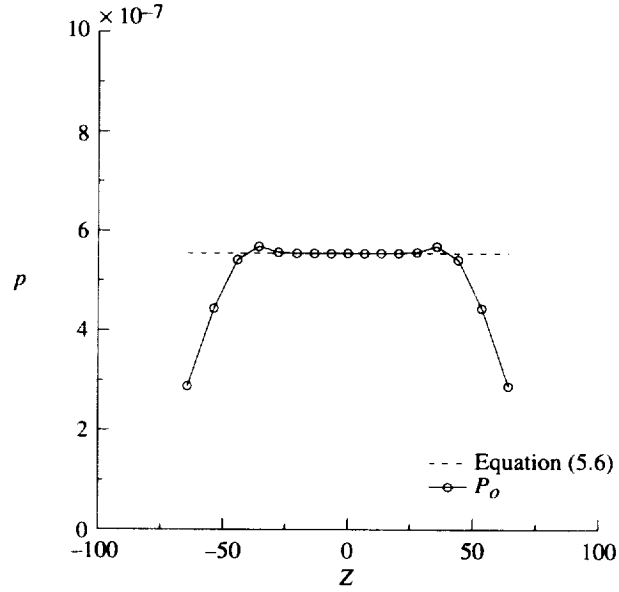

Figure 6.10. Maximum pressure with flow-acceleration direction at X = 100 in attachment-line boundary layer at R = 570 and $\omega = 0.1249$.

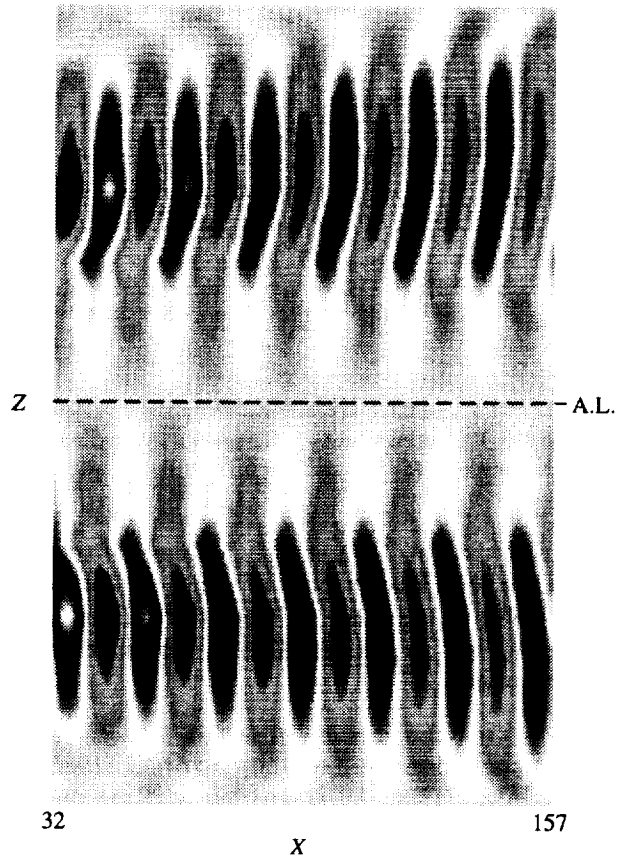

Figure 6.9. Evolution of flow-accelerated disturbance velocity w in attachment-line boundary layer at R = 570 and ω = 0.1249. Disturbance generated between X = 16 and 19.

attachment line. The results clearly show that the pressure is uniform for this type of disturbance, except at the regions where forcing is discontinued (which is expected). This uniformity supports the pressure form of Hall and Malik (1986) and thus supports the development of nonlinear subcritical growing disturbances.

6.4. Neutral-Curve Region

In parameter regimes near the neutral curve, finite Reynolds number disturbance modes are studied near the upper branch, the lower branch, and the critical point. Specifically, the simulations are conducted (in the regions shown in fig. 6.1) to verify the nonparallel theory of Hall, Malik, and Poll (1984).

For the upper branch, three simulations are performed to identify the neutral curve. The harmonic-source disturbance generator is used to generate the quasi-two-dimensional modes on the attachment line. For the Reynolds number R = 684.2, the three-dimensional simulation results are shown in figure 6.11 for various frequencies. The upper branch of the neutral curve is shown at the frequency $\omega = 0.1263$; the nonparallel theory of Hall, Malik, and Poll (1984) and the two-dimensional simulations (fig. 4.3) report that the upper branch is between $\omega = 0.1230$ and 0.1240. Although the two- and three-dimensional results yield different upper branch locations, the relative error, or difference, in the locations is only about 2 percent. This difference may be attributed to the assumption that a two-dimensional

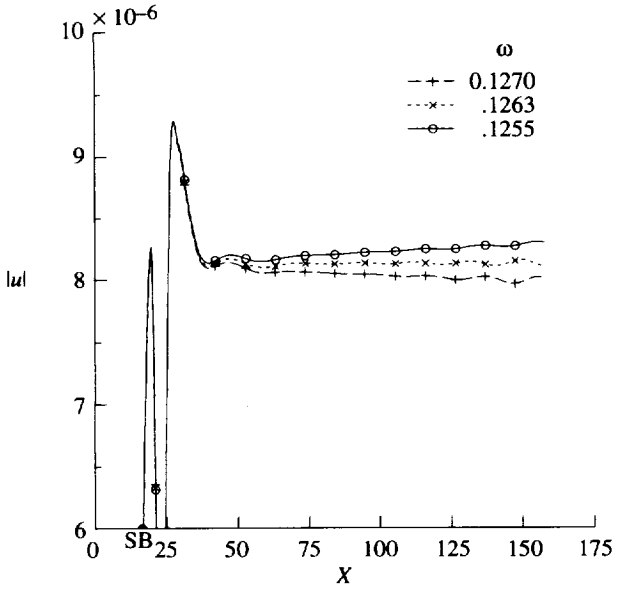

Figure 6.11. Disturbance growth and decay near branch II of curve of neutral stability for attachment-line boundary layer at $R = 684.2$.

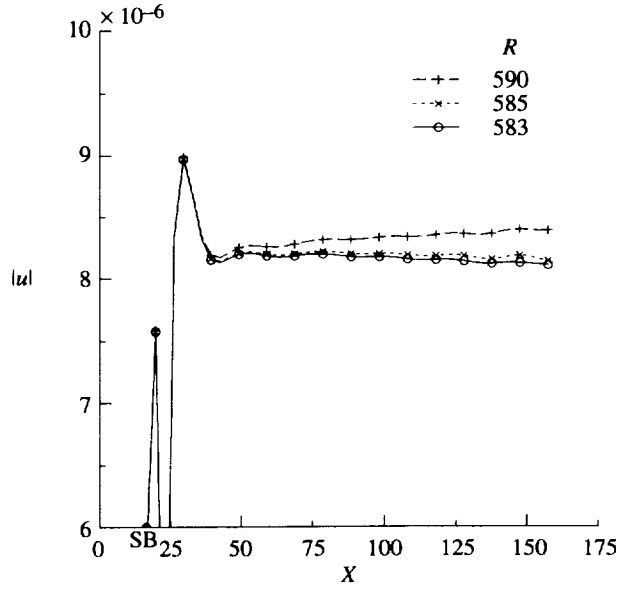

Figure 6.12. Disturbance growth and decay near critical point of curve of neutral stability for attachment-line boundary layer at $\omega = 0.1104$.

disturbance is generated from a three-dimensional harmonic source or that the three-dimensional base flow does not support pure two-dimensional disturbances.

Near the critical-point region of the neutral curve, computations are made to verify the critical point predicted by the nonparallel theory. Digitized data from the results of Hall, Malik, and Poll (1984) indicate that $R = 580$ and $\omega = 0.1104$ is the point farthest upstream at which an infinitesimal, two-dimensional disturbance becomes unstable. Although this value is not the exact critical point, this Reynolds number–frequency combination lies on the neutral curve in the region of the critical point. The computational results for disturbances in this critical-point region are shown in figure 6.12. The three-dimensional results suggest that for the frequency of $\omega = 0.1104$, the Reynolds number for neutral stability is slightly greater than $R = 585$; this represents a difference of less than 1 percent between the nonparallel theory and the simulation results.

Finally, figure 6.13 shows results from simulations performed in the vicinity of the lower branch of the neutral curve. The results indicate that for R = 684.2, the lower branch of the neutral curve is approximately at $\omega = 0.082$, which agrees with nonparallel theory.

For practical engineering purposes, the nonparallel theory of Hall, Malik, and Poll (1984) agrees with the three-dimensional simulation results in the limit of infinitesimal quasi-two-dimensional disturbances that propagate along the attachment line.

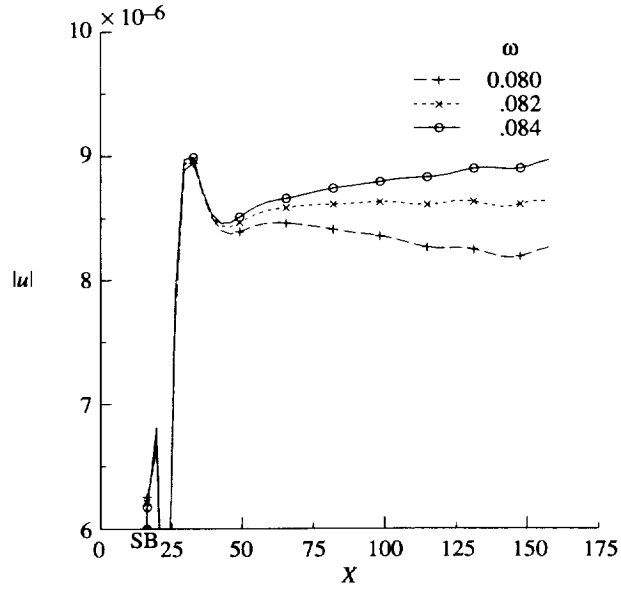

Figure 6.13. Disturbance growth and decay near branch I of curve of neutral stability for attachment-line boundary layer at $R = 684.2$.

6.5. Three-Dimensional Disturbances

To generate three-dimensional disturbances, the flow-acceleration length of the harmonic-source generator is reduced to enable a more direct transfer of energy to the velocity component w. Disturbances computed in the parameter regime described by $R = 570$ and

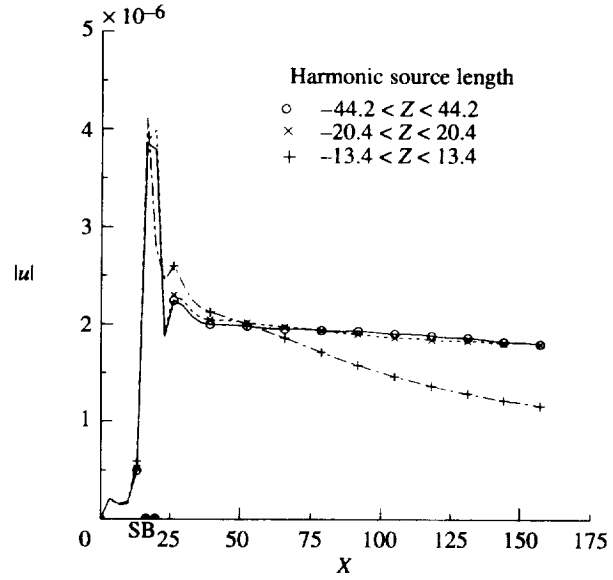

Figure 6.14. Evolution of disturbances in attachment-line boundary layer at $R = 570$ and $\omega = 0.1249$, where disturbances are generated with harmonic sources of various lengths.

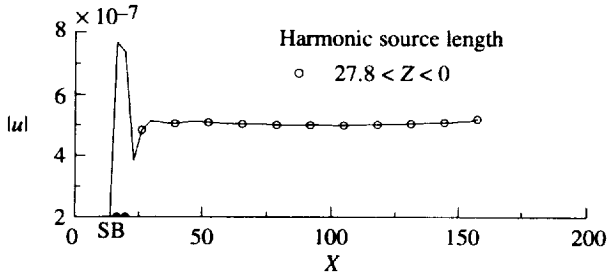

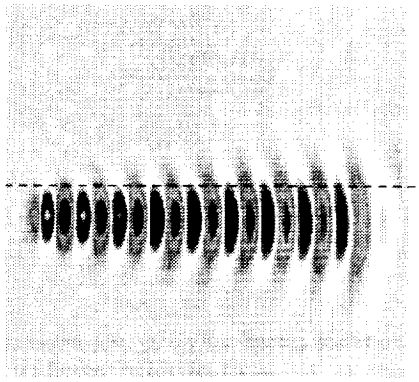

Figure 6.15. Evolution of disturbance velocity u on attachment line and top view of three-dimensional traveling wave in attachment-line boundary layer at $R = 570$ and $\omega = 0.1249$.

$\omega = 0.1249$ are shown in figure 6.14. By reducing the length of the original harmonic source from $-44.2 < Z < 44.2$ to $-20.4 < Z < 20.4$, the generated disturbance is very similar to the previous quasi-two-

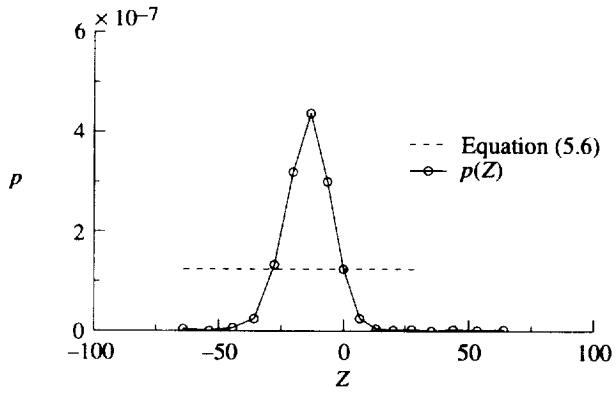

Figure 6.16. Maximum pressure variation as function of flow-acceleration direction at $X = 100$ in attachment-line boundary layer at $R = 570$ and $\omega = 0.1249$.

dimensional disturbance. However, by reducing the harmonic-source length to $-13.4 < Z < 13.4$ (one-third the original length), the generated disturbance is significantly stabilized on the attachment line. The evolution no longer represents a quasi-two-dimensional disturbance and becomes more comparable with a harmonic point source. Thus we conclude that the two-dimensional instabilities are apparently dominant on the attachment line.

Next, a harmonic-source generator is used to introduce a disturbance off the attachment line to determine the direction and rate of disturbance growth or decay. The results of a disturbance generated with a harmonic source located at $-27.8 < Z < 0.0$ are shown in figure 6.15. The top view indicates that the harmonic source generates a local almost circular pattern that evolves along the attachment line with spreading both away from and toward the attachment line. These results suggest that the flow-accelerated shear away from the attachment line has insufficient strength to deter the spreading of the disturbance toward the attachment line. Figure 6.15 also shows that the maximum-amplitude velocity u on the attachment line initially undergoes a slight decay and then continues to grow. The amplitude information along the attachment line suggests that an unstable mode is observed in the simulations; however, the top view of the flow field indicates that this amplification is caused by the wave-spreading phenomenon. The combined amplitude and visual results imply that a disturbance generated off (but near) the attachment line can supply energy to the attachment region by the spreading of the wave pattern. In turn, this energy supply may feed an unstable mode on the attachment line.

Similar to the pressure comparison in figure 6.10, the pressure for the disturbance near but off the attachment line is plotted in figure 6.16. Clearly, a zero pressure

gradient in the flow-acceleration direction does not occur for a 3D harmonic wave packet. The difference in pressure form suggests that for 3D disturbances subcritical growth is not assured based on 2D simulation results and that a full 3D nonlinear study would be warranted.

For the final simulation in this section, $R = 684.2$ and $\omega = 0.1150$ are used because the nonparallel theory predicts that infinitesimal two-dimensional disturbances are unstable on the attachment line. The disturbance is generated with a harmonic source which is positioned at $-35.6 < Z < -6.6$ (i.e., completely off the attachment line). The top view of the computed disturbance is shown in figure 6.17. As before, the disturbance evolves primarily along the attachment line, and the wave spreads both away from and toward the attachment line. Streamlines and vortex lines (determined by computing the trace of velocity and vorticity vectors) are overlaid on the disturbance pattern. These lines yield valuable information on the mean flow field properties near the attachment line. The disturbance packet follows the streamlines, and the packet spreads and evolves near the attachment line in a manner similar to packets in flat-plate boundary-layer flows. These results and the quasi-two-dimensional results suggest that the behavior of instabilities in the region on and near the attachment line can be expected to be qualitatively similar to flat-plate boundary-layer instabilities. Supporting this postulation, the trace of velocity vectors in the wall-normal–flow-acceleration plane are shown at the top of figure 6.17. The resulting pattern in a reference frame moving with the disturbance velocity is reminiscent of Kelvin cat's eyes, which are observed in the two-dimensional flat-plate boundary-layer flow.

The amplitudes of the disturbance at various Z locations are shown in figure 6.18. The component u of the disturbance has a peak amplitude initiated at $Z = -20.4$ and undergoes a strong decay along the attachment line, although the mode is shown to be unstable on the attachment line. The spread of the disturbance toward the attachment line indicates that the disturbance on the attachment line is either unstable or merely gaining energy at a rate comparable with the spreading rate. However, because the theory for two-dimensional disturbances indicates that the disturbance is unstable on the attachment line, some combination of energy transfer due to spreading and linear growth is likely. However, the more stable three-dimensional modes may rob the two-dimensional mode of enough energy to prevent flow transition along the attachment line. Note that the velocity components u at all Z locations indicate growth with distance along the attachment line, except for the location $Z = -20.4$, where decay is indicated. Spreading causes the other locations Z to receive energy, but because the location $Z = -20.4$ was the location of maximum initial amplitude and the disturbance propagates along and away from the attachment line, the location of the maximum velocity is no longer at $Z = -20.4$. This results in an observed decay at the location $Z = -20.4$. Figure 6.19 shows velocity profiles at various locations of Z at $X = 100$. As energy is transferred because of this spreading, the profiles near the attachment line undergo a distortion near the wall. This distortion leads to multiple maximums and profile shapes that deviate from the linear theory.

6.6. Asymmetric Disturbances

Recently, Lin and Malik (1994, 1995) have shown with theory that both symmetric and asymmetric instabilities are present in incompressible and compressible swept Hiemenz flow. In this section, the 3D DNS is used to validate the theoretical prediction of asymmetric modes.

The solutions posed by Lin and Malik (1994) took the form

$$\{u,v,w\}(X,Y,Z,t) = \{u,v,w\}(Y,Z)\, e^{i(\alpha X - \omega t)} \quad (6.5)$$

Substituting this form into the Navier-Stokes equations leads to a system of partial differential equations in the flow-acceleration and wall-normal directions. The boundary conditions for the boundaries Z took the following forms:

Symmetric:

$$\frac{\partial u}{\partial Z} = \frac{\partial v}{\partial Z} = w = 0 \qquad (Z = 0) \quad (6.6)$$

$$\left.\begin{aligned} \{u,v\}(Y,Z) &= \{u,v\}(Y,-Z) \\ w(Y,Z) &= -w\{Y,-Z\} \end{aligned}\right\} \qquad (Z = Z_{max}) \quad (6.7)$$

Asymmetric:

$$u = v = \frac{\partial w}{\partial Z} = 0 \qquad (Z = 0) \quad (6.8)$$

$$\left.\begin{aligned} \{u,v\}(Y,Z) &= -\{u,v\}(Y,-Z) \\ w(Y,Z) &= w\{Y,-Z\} \end{aligned}\right\} \qquad (Z = Z_{max}) \quad (6.9)$$

For the theory, Lin and Malik (1996) showed that as long as $Z_{max} \geq 2$, domain independent convergence was achieved.

For the simulations, the entire attachment-line region is included within the domain, and therefore, the boundary conditions at $Z = 0$ are not needed. Although the boundary conditions at $\pm Z_{max}$ were used to validate the theory, it was demonstrated that simple Dirichlet conditions are sufficient for boundary conditions provided $\pm Z_{max}$ is far-removed from the disturbance field.

X

Trace of velocity vectors

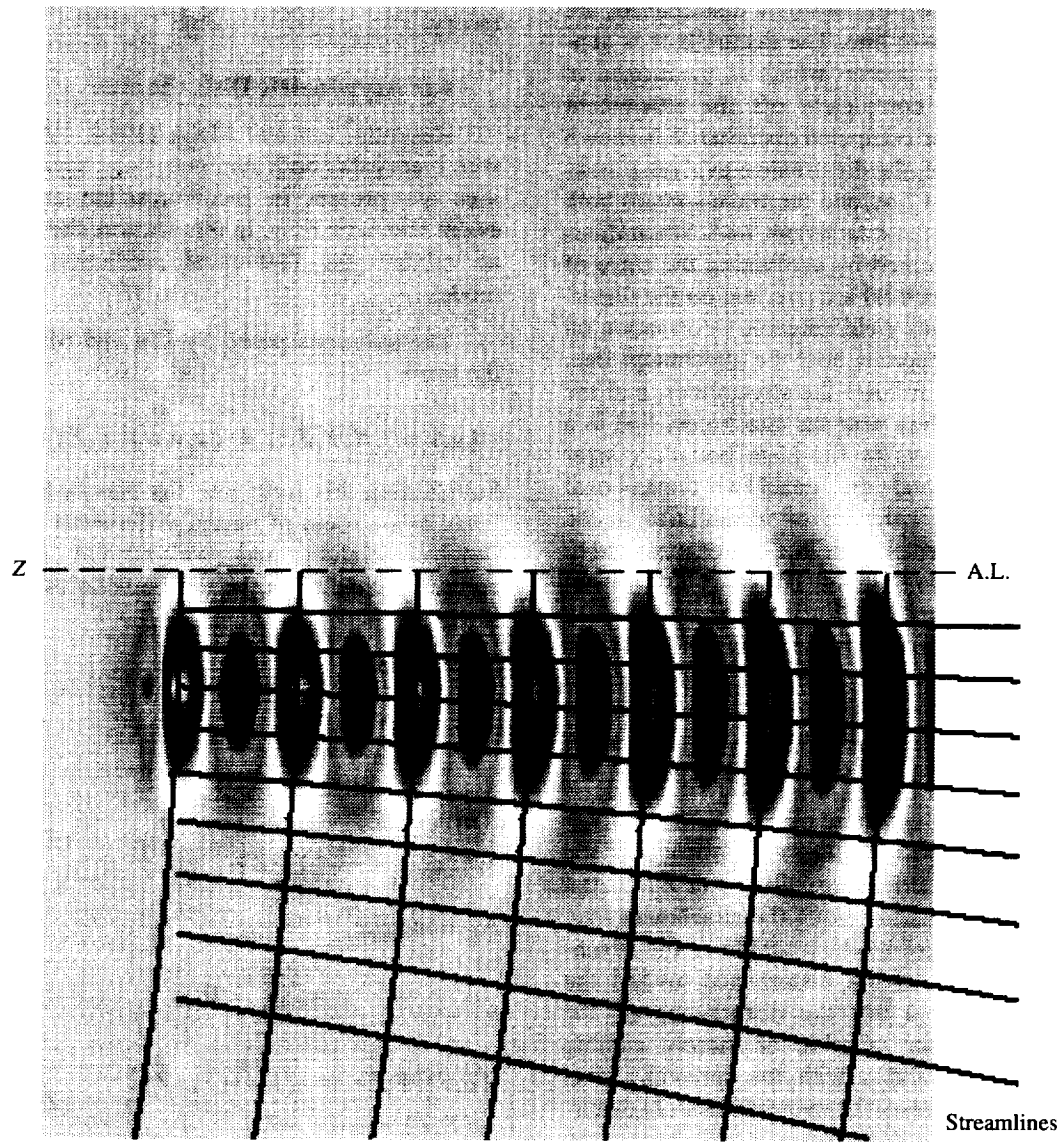

Figure 6.17. Top view of disturbance evolution in attachment-line boundary layer at $R = 684.2$ and $\omega = 0.1150$, where disturbance is generated with harmonic source near attachment line.

The theory suggests that the most unstable modes follow the sequence: symmetric (S1), asymmetric (A1), symmetric (S2), et cetera, where the growth rates of modes are S1 > A1 > S2 > A2 > S3..., without exception. This theory and modal growth ordering were recently confirmed by A. Fedorov, of Moscow Institute of Physics and Technology, using an asymptotic theory. Although according to the Fedorov analysis, the validation of a single mode implies the validation of all modes, here the first two dominant modes are simulated.

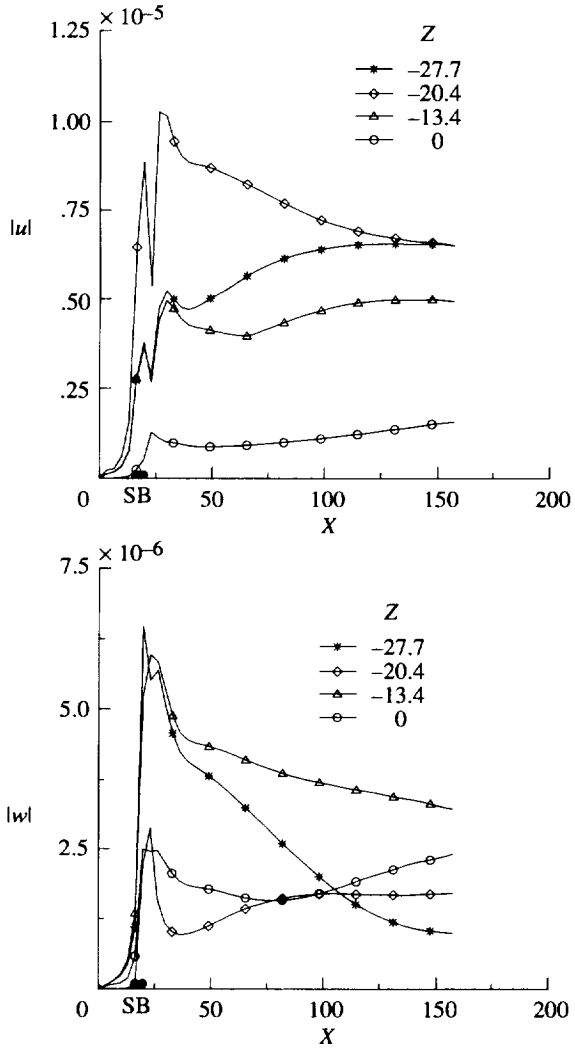

Figure 6.18. Evolution of disturbance generated off attachment line in attachment-line boundary layer at R = 684.2 and $\omega = 0.1150$. Harmonic source generated at $-35.6 < Z < -6.6$.

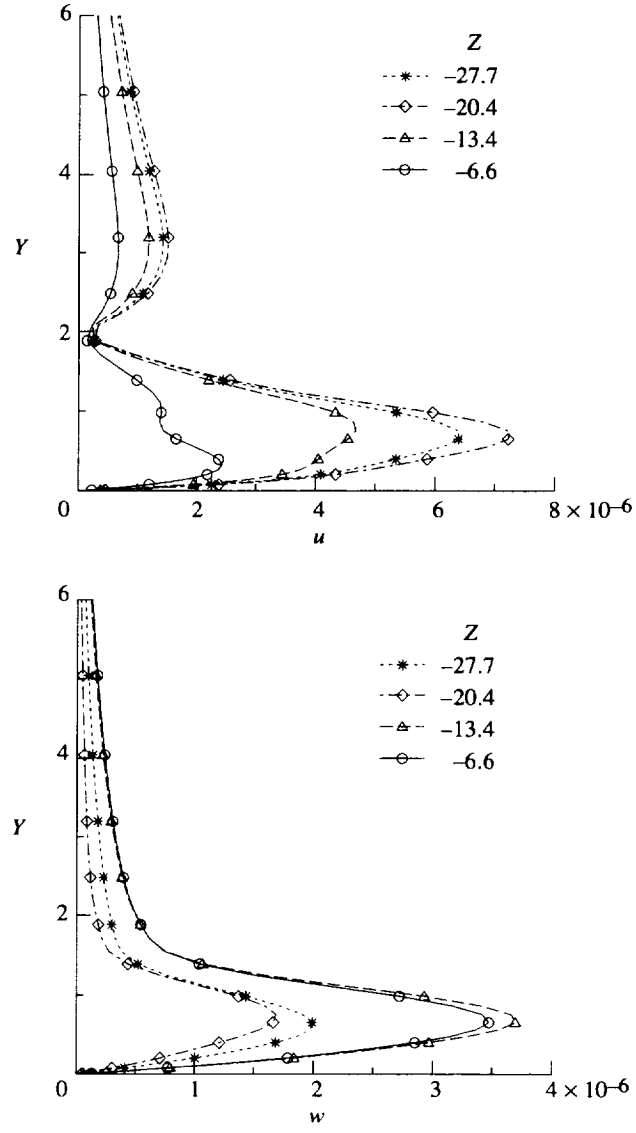

Figure 6.19. Three-dimensional disturbance velocity profiles at X = 100 near attachment line for R = 684.2 and $\omega = 0.1150$.

From the results of the Lin-Malik technique, the wave number and growth rate for the first three modes at R = 700 and $\omega = 0.1017$ are shown in table 6.1. The simulation of a pure mode will prove difficult because the discrimination of the wave numbers would be difficult. The theoretical results suggest that the previous simulations of "discrete modes" are in fact spectrally rich. To use suction and blowing to generate the S1 mode in the absence of the S2 mode would prove difficult. However, a discriminating factor can be attributed to the phase relation between the symmetric versus asymmetric modes across the attachment line and in the flow-acceleration direction. This difference is obvious from the boundary conditions for $Z = 0$ in equations (6.6) and (6.8). Hence, simulations could discriminate between symmetric and asymmetric modes.

Table 6.1. Symmetric and Asymmetric Modes for Swept Hiemenz Flow at R = 700 and $\omega = 0.1017$

Mode	α_r	α_i
S1	0.27481152	-0.226959×10^{-2}
A1	0.27515243	-0.105988×10^{-2}
S2	0.27548905	$+0.148157 \times 10^{-3}$

The simulations are performed on a grid of 661 points (≈60 points per wavelength) along the attachment line, 81 points in the wall-normal direction, and 25 points in the flow-acceleration direction. The far-field boundary is located at 40δ from the wall, the

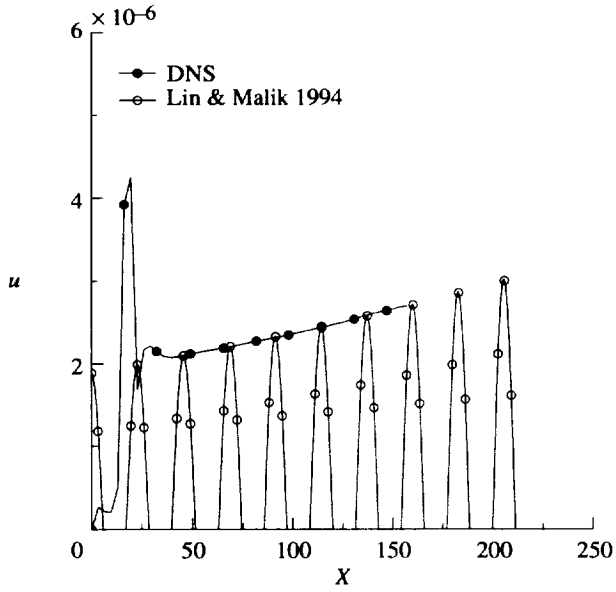

Figure 6.20. Attachment-line symmetric disturbance (S1) growth and Lin and Malik (1994) theory for three-dimensional attachment-line basic flow for $R = 700$ and $\omega = 0.1017$.

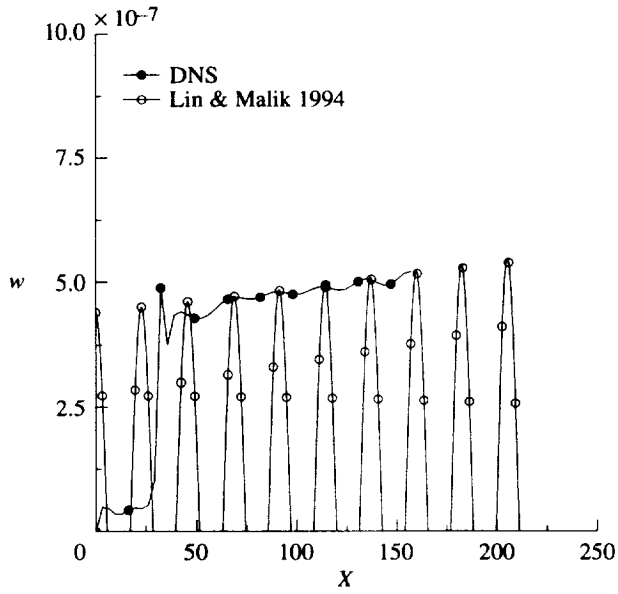

Figure 6.21. Flow-acceleration asymmetric disturbance (A1) growth and Lin and Malik (1994) theory for three-dimensional attachment-line basic flow for $R = 700$ and $\omega = 0.1017$.

computational length along the attachment line is 216δ, and the flow-acceleration boundaries are located $\pm 100\delta$. The total Cray C-90 computer cost for this simulation is 13 hr for 8 periods in time. Separately, the symmetric (S1) and the asymmetric mode (A1) are forced by using suction and blowing as before with the symmetric and

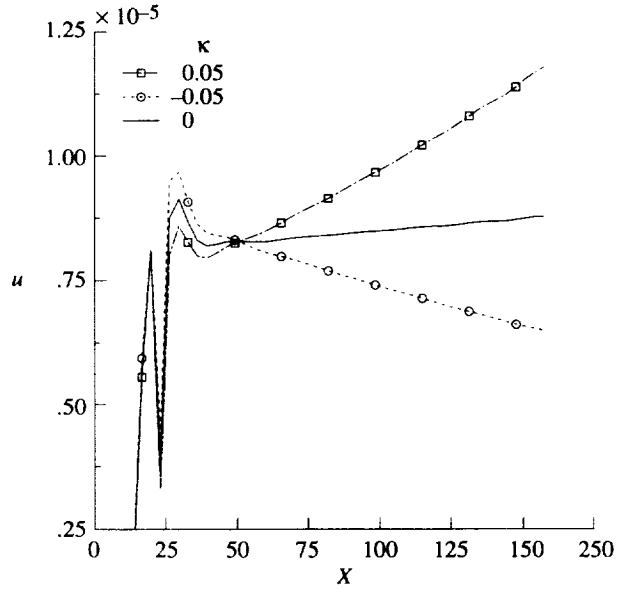

Figure 6.22. Effect of suction and blowing on growing quasi-2D symmetric disturbance in attachment-line boundary layer at $R = 684.2$ and $\omega = 0.1230$.

three-dimensional disturbances. The phase of the A1 mode in the flow-acceleration direction was determined with the Lin-Malik technique. Although the boundary conditions at $\pm Z_{max}$ were used to validate the theory, it was demonstrated that simple Dirichlet conditions are sufficient for boundary conditions provided $\pm Z_{max}$ is far-removed from the disturbance field.

In figures 6.20 and 6.21, the simulation results are compared with the wave growth rate described by the theory (listed in table 6.1). The agreement is remarkably good when considering the differences between the DNS and assumed solution form in equation (6.5). For the theory, the A1 mode has a constant wave number and growth rate in the flow-acceleration direction, whereas the simulations have a truly three-dimensional disturbance, and therefore, spectral differences in the Z-direction are inevitable in this 3D flow. To make the comparison shown in figure 6.20, the results for the simulation are averaged over the flow-acceleration stations: $Z = 0$ and ± 6. These stations were selected because, as figure 6.17 shows, the streamlines very near the attachment line are essentially aligned with the 2D attachment-line flow. The stations $Z = \pm 6$ permit a cancellation of any opposing flow-acceleration effects.

6.7. Effects of Suction and Blowing on Disturbance Growth

By changing the boundary conditions in equation (3.1) from $\kappa = 0$, steady suction ($\kappa < 0$) or blowing

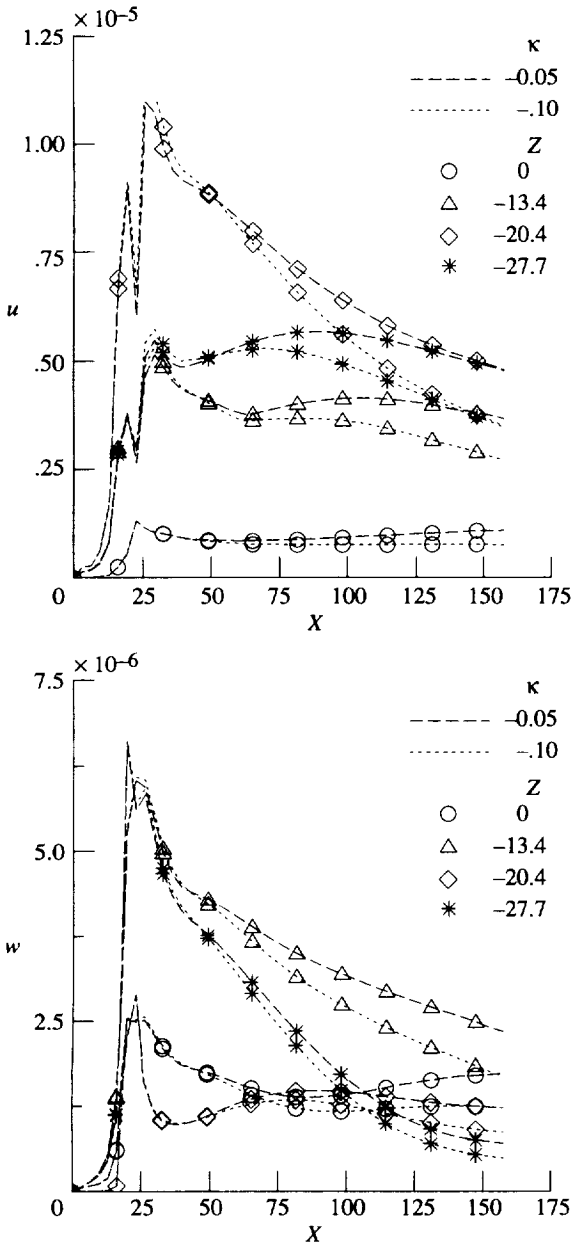

Figure 6.23. Effect of suction on evolution of disturbance generated off attachment line in attachment-line boundary layer at $R = 684.2$ and $\omega = 0.1150$. Harmonic source generated at $-35.6 < Z < -6.6$.

($\kappa > 0$) can be used to alter the growth or decay of disturbances in the attachment-line boundary-layer flow. Near the upper branch of the neutral curve, $R = 684.2$ and $\omega = 0.1230$ are used for the simple test case of linear stability with suction and blowing. Shown in figure 6.22, the results of the quasi-two-dimensional disturbance generated with the elongated harmonic source ($-44.2 < Z < 44.2$) indicate that suction stabilizes the disturbance and blowing destabilizes the disturbance; this agrees with the theoretical results by Hall, Malik, and Poll (1984) and the two-dimensional simulation results in figure 4.12.

The results for the three-dimensional disturbance generated with a harmonic source of length $-35.6 < Z < -6.6$ at $R = 684.2$ and $\omega = 0.1150$ indicated growth in the energy on the attachment line (fig. 6.18). Because two-dimensional disturbances at this Reynolds number and frequency are linearly unstable on the attachment line, the presence of energy should lead to disturbance growth. Computations with suction are used to evaluate disturbance stabilization on and near the attachment line. Clearly, figure 6.23 shows that suction stabilizes the disturbances located both on and off the attachment line.

6.8. Region of Subcritical Disturbance Growth

The weakly nonlinear theory and Fourier-based simulations by Hall and Malik (1986) and the results of section 5.3 reveal that a region of nonlinear subcritical growth exists for large-amplitude disturbances that evolve on the attachment line of a three-dimensional boundary-layer flow. Because the 3D results shown in figure 6.6 indicate that much larger harmonic-source amplitudes are required to initiate large-amplitude disturbances and because of the large computational costs involved to resolve this nonlinear phenomenon, three-dimensional simulations of large-amplitude instabilities were not attempted in this paper.

7. Concluding Remarks

In this study, results are presented for the spatial direct numerical simulations (DNS) of the two-dimensional (2D) and three-dimensional (3D) disturbances that propagate along the attachment line of a swept Hiemenz flow. With a quasi-parallel base-flow approximation, the small-amplitude disturbances were shown to grow and decay in agreement with linear stability theory. The true swept Hiemenz base flow leads to a destabilization of the flow, which agrees with the nonparallel theory of Hall, Malik, and Poll. Furthermore, the effect of steady suction and blowing on small-amplitude disturbances was documented with direct numerical simulation (DNS). In agreement with the results of Hall, Malik, and Poll, suction stabilizes and blowing destabilizes the small-amplitude disturbances.

A computational approach was described, which permits simulations of disturbances that evolve in flows where the periodic assumption is invalid. Small-amplitude quasi-two-dimensional disturbances, computed in a quasi-parallel base flow, were shown to grow and decay in agreement with two-dimensional linear stability theory. For complete swept Hiemenz flow, the flow

is destabilized in comparison with those from both linear stability theory and two-dimensional simulation results.

The neutral-curve location predicted by the nonparallel theory of Hall, Malik, and Poll agreed well with the three-dimensional simulation results in the limit of infinitesimal quasi-two-dimensional disturbances, which propagate along the attachment line. Furthermore, the effects of both steady suction and blowing on small-amplitude disturbances were documented with direct numerical simulation. In agreement with the results of Hall, Malik, and Poll, suction damps small-amplitude disturbances, and blowing amplifies these disturbances.

For the parameter regions studied here, instabilities that are generated from harmonic sources located off the attachment line spread both toward and away from the attachment line. Because of this spreading, energy from the initial disturbance is transferred to the attachment-line instabilities; however, suction stabilizes these instabilities. Furthermore, three-dimensional instabilities were more stable than two-dimensional, or quasi-two-dimensional, instabilities.

Subcritical nonlinear disturbance growth was detected with a weakly nonlinear theory and computations by Hall and Malik. Later, DNS studies by Theofilis and Jiménez et al. failed to find this nonlinear disturbance growth. The present 2D and 3D simulations have detected nonlinear subcritical disturbance growth; these results support the former theoretical and computational results of Hall and Malik. Based on the present results, the computations by Theofilis may not have achieved subcritical growth because the forcing amplitudes were apparently too small. Furthermore, Jiménez et al. apparently used a different disturbance pressure form in the flow-acceleration direction. The present study showed that this assumed variation in pressure leads to a decaying subcritical mode, which qualitatively agrees with the results of Jiménez et al. These results suggest that the reason for the discrepancy may evidently be attributable to differing disturbance pressure forms. The 3D DNS results tend to support the pressure form used by Hall and Malik for the types of disturbances considered. The difference in pressure form suggests that for 3D disturbances subcritical growth is not assured based on 2D simulation results and that a full 3D nonlinear study would be warranted.

Furthermore, the DNS results demonstrate that steady suction stabilizes the otherwise nonlinearly growing disturbances. No nonlinear growing disturbances were detected near branch I of the neutral curve; however, nonlinear neutral-like states were found near branch I.

Finally, the simulation results of 3D symmetric and asymmetric disturbances were shown to be in agreement with the 2D-eigenvalue calculations of Lin and Malik and theory of Fedorov.

Although the present study has served to resolve the previous discrepancy surrounding the subcritical growing disturbances, the results have not explained the physics of the flow between the known limit of linear instability $R_\theta \cong 245$ and the bypass (or turbulence) limit of $R_\theta \cong 100$. The present nonlinear results suggest that the linear critical Reynolds can be slightly reduced due to nonlinear effects; however, the true swept-wing bypass problem likely involves potentially large and multi-frequency–multi-wave-number 3D disturbances. Hence, the explanation for bypass transition will involve these multiple modes, which may be generated off the attachment line. Furthermore, the fully 3D DNS results have shown that disturbance packets generated off but near the attachment line can transfer energy to the attachment-line region.

Hall and Seddougui studied oblique waves and their interaction in attachment-line flow at the large Reynolds number limit. They note that close to the attachment line a small band of destabilized oblique modes appear, interact with the 2D mode, and cause a breakdown of the 2D mode. Furthermore, Lin and Malik have shown that many symmetric and asymmetric disturbances exist with the attachment-line region. Although these symmetric and asymmetric disturbances are linearly stable in the subcritical region outlined by Hall and Malik, perhaps some combination of small (but finite) amplitude disturbances may cause catastrophic breakdown scenarios in the subcritical region. A future study which would involve multiple combinations of finite-amplitude 2D and 3D symmetric and asymmetric modes in the subcritical region may lead to a better understanding of the Reynolds number region between the linear instability and point where turbulence is suppressed.

NASA Langley Research Center
Hampton, VA 23681-0001
October 16, 1996

8. References

Arnal, D. 1992: Boundary Layer Transition: Prediction, Application to Drag Reduction. *Special Course on Skin Friction Drag Reduction*, AGARD Rep. 786.

Canuto, Claudio; Hussaini, M. Yousuff; Quarteroni, Alfio; and Zang, Thomas A. 1988: *Spectral Methods in Fluid Dynamics*. Springer-Verlag.

Cumpsty, N. A.; and Head, M. R. 1969: The Calculation of the Three-Dimensional Turbulent Boundary Layer—III. *Aeronaut. Q.*, vol. 20, pp. 99–113.

Danabasoglu, G.; Biringen, S.; and Streett, C. L. 1990: Numerical Simulation of Spatially-Evolving Instability Control in Plane Channel Flow. AIAA-90-1530.

Danabasoglu, G.; Biringen, S.; and Streett, C. L. 1991: Spatial Simulation of Instability Control by Periodic Suction Blowing. *Phys. Fluids A*, vol. 3, pp. 2138–2147.

El-Hady, N. M.; and Nayfeh, A. H. 1978: Nonparallel Stability of Two-Dimensional Heated Boundary Layer Flows. *Proceedings of the Twelfth Symposium on Naval Hydrodynamics*, National Academy of Sciences—National Research Council.

Gad-el-Hak, Mohamed; and Bushnell, Dennis M. 1991: Separation Control—Review. *J. Fluids Eng.*, vol. 113, pp. 5–30.

Gaster, M. 1965: A Simple Device for Preventing Turbulent Contamination on Swept Leading Edges. *J. R. Aeronaut. Soc.*, vol. 69, no. 659, pp. 788–789.

Gaster, M. 1967: On the Flow Along Swept Leading Edges. *Aeronaut. Q.*, vol. XVIII, pt. 2, pp. 165–184.

Gaster, M. 1974: On the Effects of Boundary-Layer Growth on Flow Stability. *J. Fluid Mech.*, vol. 66, pp. 465–480.

Gregory, N.; and Love, E. M. 1965: *Laminar Flow on a Swept Leading Edge: Final Progress Report*. NPL Memo. No. 26, British A.R.C.

Hall, P.; Malik, M. R.; and Poll, D. I. A. 1984: On the Stability of an Infinite Swept Attachment Line Boundary Layer. *Proc. R. Aeronaut. Soc. (London), ser. A*, vol. 395, no. 1809, pp. 229–245.

Hall, P.; and Malik, M. R. 1986: On the Instability of a Three-Dimensional Attachment-Line Boundary Layer—Weakly Nonlinear Theory and a Numerical Approach. *J. Fluid Mech.*, vol. 163, pp. 257–282.

Hall, Philip; and Seddougui, Sharon O. 1990: Wave Interactions in a Three-Dimensional Attachment-Line Boundary Layer. *J. Fluid Mech.*, vol. 217, pp. 367–390.

Hiemenz, K. 1911: Die Grenzschicht an einem in der gleichförmigen Flüssigkeitsstrom eingetauchten geraden Kreeiszylinder. *Dinglers Polytech. J.*, vol. 326, p. 322.

Jiménez, Javier; Martel, Carlos; Agüí, Juan C.; and Zufiria, Juan A. 1990: *Direct Numerical Simulation of Transition in the Incompressible Leading Edge Boundary Layer*. Tech. Note ETSIA /MF-903, School of Aeronaut., Universidad Politécnica Madrid.

Joslin, Ronald D.; Streett, Craig L.; and Chang, Chau-Lyan 1992: *Validation of Three-Dimensional Incompressible Spatial Direct Numerical Simulation Code—A Comparison With Linear Stability and Parabolic Stability Equation Theories for Boundary-Layer Transition on a Flat Plate*. NASA TP-3205.

Joslin, R. D.; Streett, C. L.; and Chang, C.-L. 1993: Spatial Direct Numerical Simulation of Boundary-Layer Transition Mechanisms—Validation of PSE Theory. *Theor. & Comput. Fluid Dyn.*, vol. 4, no. 6, pp. 271–288.

Koerner, H.; Horstmann, K. H.; Koester, H.; Quast, A.; and Redeker, G. 1987: Laminarization of Transport Aircraft Wings—A German View. AIAA-87-0085.

Lin, R. S.; and Malik, M. R. 1994: The Stability of Incompressible Attachment-Line Boundary Layers—A 2D-Eigenvalue Approach. AIAA-94-2372.

Lin, R. S.; and Malik, M. R. 1995: Stability and Transition in Compressible Attachment-Line Boundary-Layer Flow. SAE Paper 952041.

Lin, R. S.; and Malik, M. R. 1996: On the Stability of Attachment-Line Boundary Layers—Part 1. *J. Fluid Mech.*, vol. 311, p. 239.

Lynch, Robert E.; Rice, John R.; and Thomas, Donald H. 1964: Direct Solution of Partial Difference Equations by Tensor Product Methods. *Numer. Math.*, vol. 6, pp. 185–199.

Maddalon, D. V.; Collier, F. S., Jr.; Montoya, L. C.; and Putnam, R. J. 1990: Transition Flight Experiments on a Swept Wing With Suction. *Laminar-Turbulent Transition*, D. Arnal and R. Michel, eds., Springer-Verlag, pp. 53–62.

Pfenninger, W. 1965: *Recent Developments in Boundary Layer Research—Part IV*. AGARDograph-97, Pt. IV.

Pfenninger, W.; and Bacon, J. W., Jr. 1969: Amplified Laminar Boundary Layer Oscillations and Transition at the Front Attachment Line of a 45° Swept Flat-Nosed Wing With and Without Boundary Layer Suction. *Viscous Drag Reduction*, C. Sinclair Wells, ed., Plenum Press, pp. 85–105.

Poll, D. I. A. 1979: Transition in the Infinite Swept Attachment Line Boundary Layer. *Aeronaut. Q.*, vol. 30, pp. 607–629.

Poll, D. I. A. 1980: Three-Dimensional Boundary Layer Transition Via the Mechanisms of Attachment Line Contamination and Cross Flow Instability. *Laminar-Turbulent Transition*, R. Eppler and H. Fasel, eds., Springer-Verlag, pp. 253–262.

Poll, D. I. A. 1985: Some Observations of the Transition Process on the Windward Face of a Long Yawed Cylinder. *J. Fluid Mech.*, vol. 150, pp. 329–356.

Reed, H. L.; and Saric, W. S. 1986: Stability and Transition of Three-Dimensional Flows. *Proceedings of the 10th U.S. National Congress of Applied Mechanics*, ASME, pp. 457–468.

Spalart, P. R. 1989: Direct Numerical Study of Leading-Edge Contamination. *Fluid Dynamics of Three-Dimensional Turbulent Shear Flows and Transition*, AGARD-CP-438, pp. 5-1–5-13.

Streett, C. L.; and Hussaini, M. Y. 1991: A Numerical Simulation of the Appearance of Chaos in Finite Length Taylor-Couette Flow. *Appl. Numer. Math.*, vol. 7, no. 1, pp. 41–71.

Streett, C. L.; and Macaraeg, M. G. 1989: Spectral Multi-Domain for Large-Scale Fluid Dynamic Simulations. *Int. J. Appl. Numer. Math.*, vol. 6, pp. 123–139.

Theofilis, Vassilios 1993a: Numerical Experiments on the Stability of Leading Edge Boundary Layer Flow—A Two-Dimensional Linear Study. *Int. J. Numer. Methods Fluids*, vol. 16, no. 2, pp. 153–170.

Theofilis, Vassilios 1993b: A Spectral Velocity-Vorticity Algorithm for the Solution of the Incompressible Navier-Stokes Equations. *Numerical Methods in Laminar and Turbulent Flow*, Volume VIII, Part 1, C. Taylor, ed., Pineridge Press, pp. 801–811.

Tuttle, Marie H.; and Maddalon, Dal V. 1982: *Laminar Flow Control (1976–1982)—A Selected Annotated Bibliography*. NASA TM-84496.

Williamson, J. H. 1980: Low-Storage Runge-Kutta Schemes. *J. Comput. Phys.*, vol. 35, no. 1, pp. 48–56.

REPORT DOCUMENTATION PAGE

Form Approved
OMB No. 0704-0188

1. AGENCY USE ONLY *(Leave blank)*	2. REPORT DATE	3. REPORT TYPE AND DATES COVERED
	February 1997	Technical Paper

4. TITLE AND SUBTITLE
Direct Numerical Simulation of Evolution and Control of Linear and Nonlinear Disturbances in Three-Dimensional Attachment-Line Boundary Layers

5. FUNDING NUMBERS
WU 505-59-50-02

6. AUTHOR(S)
Ronald D. Joslin

7. PERFORMING ORGANIZATION NAME(S) AND ADDRESS(ES)
NASA Langley Research Center
Hampton, VA 23681-0001

8. PERFORMING ORGANIZATION REPORT NUMBER
L-17578

9. SPONSORING/MONITORING AGENCY NAME(S) AND ADDRESS(ES)
National Aeronautics and Space Administration
Washington, DC 20546-0001

10. SPONSORING/MONITORING AGENCY REPORT NUMBER
NASA TP-3623

11. SUPPLEMENTARY NOTES

12a. DISTRIBUTION/AVAILABILITY STATEMENT
Unclassified–Unlimited
Subject Category 02
Availability: NASA CASI (301) 621-0390

12b. DISTRIBUTION CODE

13. ABSTRACT *(Maximum 200 words)*

Spatially evolving linear and nonlinear disturbances in a three-dimensional (3D) attachment-line boundary layer are computed by direct numerical simulation of the unsteady, incompressible Navier-Stokes equations. Previously, a weakly nonlinear theory and computation revealed a high wave-number region of subcritical disturbance growth, which is a region where linear theory predicts the decay of small-amplitude disturbances. More recent computations have failed to achieve this subcritical growth. The present computational results duplicate and explain both subcritically growing and decaying disturbances and resolve the previous theoretical and computational discrepancy. The present results demonstrate that steady suction can be used to stabilize disturbances that otherwise grow subcritically along the attachment line. However, true 3D disturbances are more likely in practice. Disturbances generated off (but near) the attachment line are shown to spread both away from and toward the attachment line as they evolve. Furthermore, these disturbances generated near the attachment line can supply energy to attachment-line instabilities, but the results show that suction can be used to stabilize these instabilities. Finally, symmetric and asymmetric disturbance growth predicted by a two-dimensional-eigenvalue approach is demonstrated to agree with the DNS results.

14. SUBJECT TERMS	15. NUMBER OF PAGES
Direct numerical simulation; Attachment-line boundary-layer transition	39
	16. PRICE CODE A03

17. SECURITY CLASSIFICATION OF REPORT	18. SECURITY CLASSIFICATION OF THIS PAGE	19. SECURITY CLASSIFICATION OF ABSTRACT	20. LIMITATION OF ABSTRACT
Unclassified	Unclassified	Unclassified	

NSN 7540-01-280-5500

Standard Form 298 (Rev. 2-89)
Prescribed by ANSI Std. Z39-18
298-102